LA-4426

c.3

LOS ALAMOS SCIENTIFIC LABORATORY
of the
University of California

LOS ALAMOS • NEW MEXICO

Flash X-Ray Observation of the Flow Behind a Detonation Wave

UNITED STATES
ATOMIC ENERGY COMMISSION
CONTRACT W-7405-ENG 36

This report expresses the opinions of the author or authors and does not necessarily reflect the opinions or views of the Los Alamos Scientific Laboratory.

Printed in the United States of America. Available from
National Technical Information Service
U. S. Department of Commerce
Springfield, Virginia 22151
Price: Printed Copy $3.00; Microfiche $0.65

Written: June 1970
Distributed: April 1971

LA-4426
UC-34, PHYSICS
TID-4500

LOS ALAMOS SCIENTIFIC LABORATORY
of the
University of California
LOS ALAMOS • NEW MEXICO

Flash X-Ray Observation of the Flow Behind a Detonation Wave

by

W. C. Rivard
Douglas Venable

CONTENTS

FLASH X-RAY OBSERVATION OF THE FLOW BEHIND A DETONATION WAVE

by

W. C. Rivard

and

Douglas Venable

ABSTRACT

The flow field behind a plane detonation wave in Composition B-3 (60% RDX, 40% TNT, ρ_o = 1.730 g/cm^3) is examined by radiographically observing the motion of 12.5-μm-thick metal foils placed between slabs of explosive 10 by 10 by 0.635 cm. The motion of the foils is observed along the centerline of the explosive-foil sandwich by a sequence of radiographs over a range of 5 to 10 cm of run. The final position of each foil as a function of its initial position and time is sufficient to determine the density, particle velocity, pressure, and internal energy with no a priori assumption of the equation of state. The data demonstrate to a very good approximation that the flow following the detonation wave is self-similar. The density distribution between the detonation front and the plane wave initiator is determined to within ±0.01 g/cm^3 and the pressure distribution to within ±4 kbar. The Chapman-Jouguet state is described by a pressure and detonation wave velocity of 275 ±4 kbar and 7.886 ±.008/μsec, respectively, which correspond to a density of 2.32 ±.01 g/cm^3 and a gamma of 2.92 ±.05. Pressure, density, and gamma decrease monotonically from Chapman-Jouguet values to 132 ±2 kbar, 1.72 ±.01 g/cm^3, and 1.69 ±.05, respectively, at the end of the Taylor wave. These results are compared with calculations using various calibrated equations of state.

I. INTRODUCTION

Virtually all our understanding of detonation phenomena and the state parameters of the detonation products of condensed high explosives has been derived from and supported inferentially by observations of detonation wave velocity and the motion of surfaces of objects, such as metal plates and cylinders near, or in contact with, the explosive. By today's standards, the motion of explosive-driven objects can be measured so precisely that errors of measurement scarcely affect interpretation of the observations. Interpretation of the detonation processes by means of these techniques requires an understanding of detonation wave impact and the effects of the expanding reaction products on the driven objects. The apparent circularity of this argument vanishes if the shock properties of the driven materials are well understood. This is now accepted as the case because of the thoroughness with which the Hugoniot states of many materials have been examined. However, this technique of inquiring into the mechanisms of detonation is by no means unique. Other experimentalists are studying the regions behind a detonation wave to further understanding of the same events. Some have used embedded conductors which, when moved in a magnetic field by the detonation products, induce an electric signal that is proportional to the velocity of the conductor; hence, particle velocity is measured.[1]

Some have employed the older method of flash radiography.[2-4]

Flash radiography today provides a precise measurement of the spatial distribution of mass density behind strong shocks such as detonation waves; in this work the density distribution is determined to within ±.01 g/cm^3. (All ± values quoted in this report are standard deviations unless otherwise noted.) A time sequence of these measurements describes the entire flow field behind a detonation wave and, therefore, describes directly how objects are driven. Interpretation of detonation processes from these observations should complement the interpretations from other techniques. The experimental variant peculiar to this work is the use of precisely located, radiographically observable, metal foils embedded as a sandwich within a high explosive charge. The foils are placed parallel to the plane detonation wave. The essence of the experiment is that the foils, acting as identifying tags on "particles" in the medium, are observed first in their initial positions and then later when the detonation wave has traveled a distance X. Relative changes in the foil positions provide a direct measure of the spatial density distribution. The temporal distribution can also be determined if one has suitably reproducible high explosive systems so that a meaningful sequence of shots can be made. In this case, the particle velocity distribution is also obtainable as a function of space and time. The attractiveness of this approach lies in the fact that the interpretation of the measurements depends only upon the completeness of the conservation equations and, of course, the ubiquitous errors of measurements and calculations, assuming the suitability of the data carrying vehicles, i.e., the foils and the detonation front.

The experiment is described in detail and the data are tabulated in Sec. II. The final position, x_f, of each foil as a function of the initial position, x_i, and the detonation front position, X, together with the detonation velocity as a function of front position is sufficient to determine the density, particle velocity, pressure, and internal energy from the one-dimensional Euler equations with no a priori assumption of the equation of state. The appropriate equations are given in Sec. IIIA. To calculate any flow variable, we must first obtain an analytic description of the data. We begin by seeking an analytic expression for $x_f(x_i,X)$ within the context of the classical model of detonation, i.e., an instantaneous Chapman-Jouguet[5] detonation followed by a centered simple wave (Taylor wave[6]). Several analytic expressions involving only two parameters are found and the extent of the Taylor wave region is determined. An expression representative of the mean is selected and the complete flow is calculated. This flow is taken as a standard and calculations using various calibrated equations of state (the γ-law calibrated by Deal,[7] the BKW-HOM calibrated by Mader,[8] and the JWL calibrated by Lee, Hornig, and Kury[9]) are compared to it. This work is the topic of Sec. IIIB.

II. EXPERIMENTAL METHOD

Illustrations of a typical experimental assembly, represented schematically in Fig. 2.1a and radiographically in Fig. 2.1b, show features germane to data collection and analysis. The high explosive specimen, in the form of a right parallelepiped, consists of a sandwich of precisely machined blocks with a 12.5-μm-thick tantalum foil between adjacent pieces. A plane wave generator is used to initiate the charge so that the resulting detonation wave is parallel to the plane of each foil.

The basic measurables of this experiment are the initial position, x_i, of each foil; the final position, x_f; the detonation wave velocity, D; the excursion of the detonation wave, X; and the time, t. All spatial positions are referred to the initially undisturbed interface between the plane wave generator and the specimen.

An observable region of one-dimensional flow behind the detonation wave is shown in Fig. 2.2. Within this region the foils remain parallel, as yet undisturbed by incoming lateral waves at the time of the radiograph. The position of the fronts of the incoming lateral rarefaction waves (indicated by kinks in the foils) can be mapped by this technique.

If, instead of a simple sandwich of parallel foils, one fabricates an experiment in which the foil pattern appears as a grid, he could also follow the intersections of the grid lattice as "mass points" in two- and three-dimensional flow. Indeed,

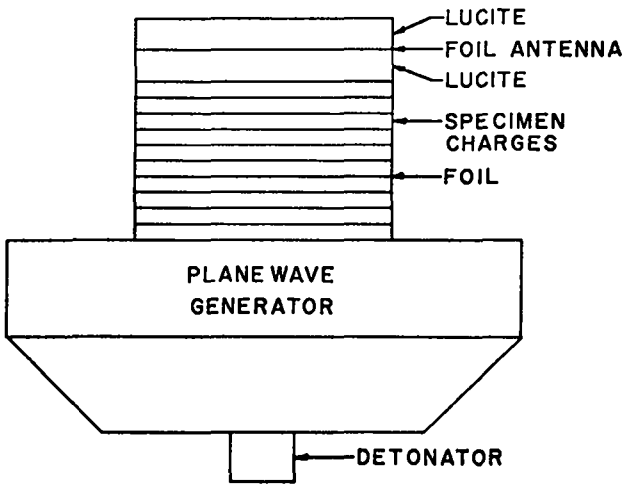

Fig. 2.1a. Schematic of typical experimental assembly.

Fig. 2.1b. Static radiograph of Shot NW-435. Wood cross-piece on top of Lucite is part of clamping mechanism that holds high explosive assembly together.

if one simply superposes the radiographs of Fig. 2.3 he would have the analog of this arrangement for a two-dimensional case. Development of this technique for two-dimensional flow is presently under investigation.

The experimental arrangement employed is depicted in Fig. 2.4. A dimensionally small source of x-rays, of the order of one millimeter in diameter, is used to cast a sharp shadow image of the object containing the embedded foils upon a photographic film. Radiation pulse lengths of 0.1 μsec with fluxes as low as 25 R, measured at 1 m from the source, are adequate to produce good contrasting images when the source-to-object distance is 3 m and the object-to-film distance is 0.7 m.

The flash radiographic techniques employed for these experiments are adequately described in Ref. 4. Since then, the capability of the PHERMEX facility has been expanded to markedly improve space and time resolutions.

Each experimental assembly uses a plane wave generator to drive a specimen of Composition B-3 (60% RDX, 40% TNT by weight). Deviations from the nominal 60% RDX component are less than 1.5%. The inner element of the plane wave driver is a nominal 20 cm diam by 8 cm long cone-shaped piece of Baratol. This initiating system is sufficiently larger in cross section than the specimen charges that the problem of decay zones[10] is unimportant. Each plane wave generator, referred to hereafter as a P-081 driver, is selected from the same production lot to minimize variations among units. The specimen charges are slabs, 10 cm by 10 cm in cross section. Charge lengths of up to 10 cm are fabricated by stacking the 0.635-cm-thick slabs. Tantalum foils 12.5 μm thick are placed between adjacent slabs and serve as the "particles" to be observed. The foils are all taken from the same roll and their total mass in any assembly is less than 2% of the total mass of the specimen charges. The slabs are machined to tolerances of ±0.005 cm in parallelism, ±0.0125 cm in thickness, and ±0.025 cm in other linear dimensions. Individual pieces are selected and oriented on the basis of both dimensions and parallelism so that tolerance build-up is virtually nonexistent. Selection on the basis of density (1.730 ±0.001 g/cm^3) is also made. Each sandwich of high explosive slabs and foils is clamped against the surface of the plane wave generator.

Prior to firing, the position of each foil with respect to the driver-Composition B-3 interface is determined by a precision cathetometer. These positions are compared with those observed on the static radiograph to provide the value of image magnification needed for interpreting the corresponding dynamic radiograph. Films are read directly without subsequent photographic reproductions.

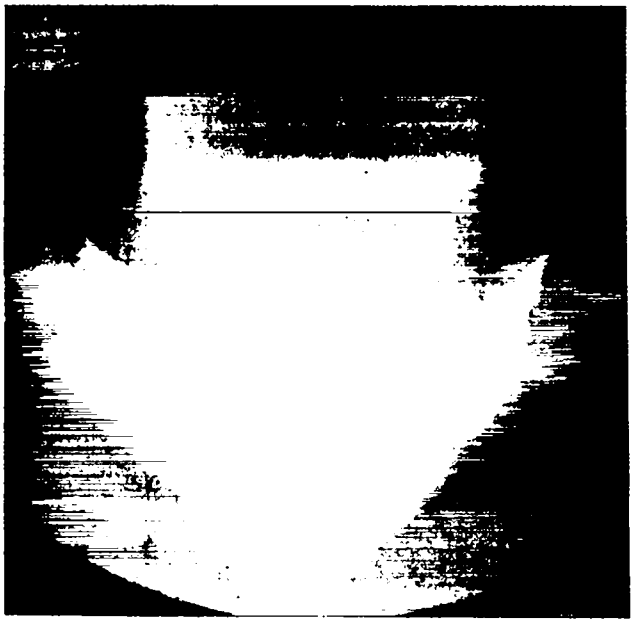

Fig. 2.2. Dynamic radiograph of NW-435.

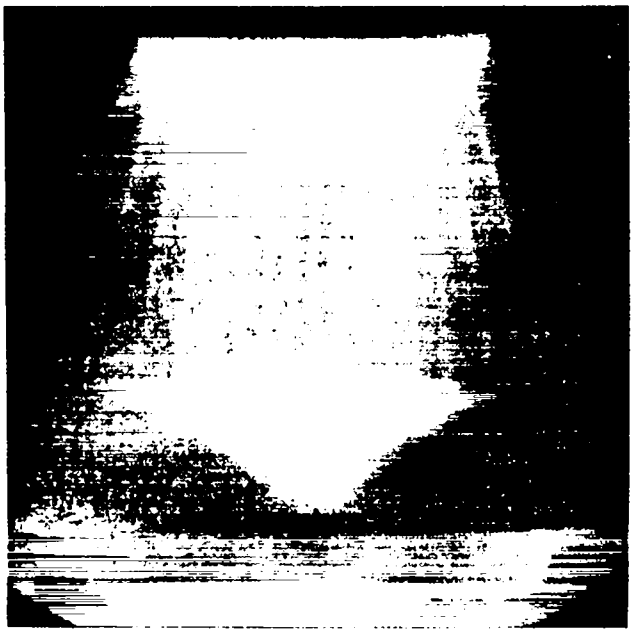

Fig. 2.3a. Dynamic radiograph of another experiment in which plane of foils is normal to detonation wave front. Wave has run almost 100 mm.

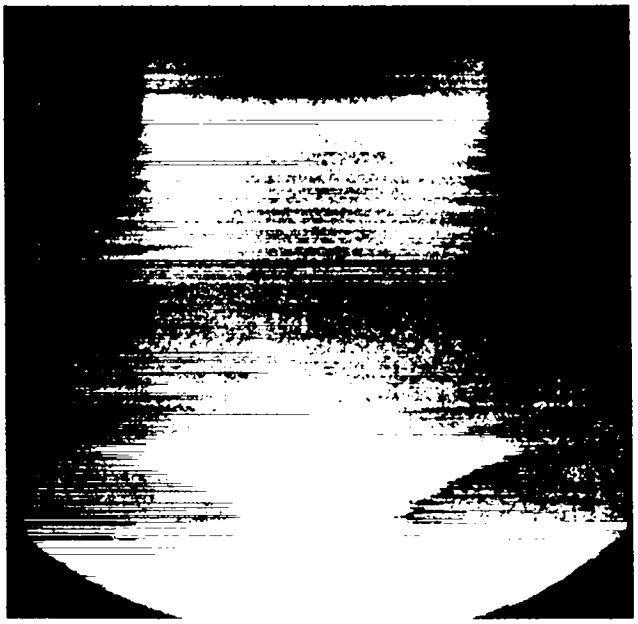

Fig. 2.3b. Dynamic radiograph of similar experment but with plane of foils parallel to detonation wave front. Wave has run almost 100 mm.

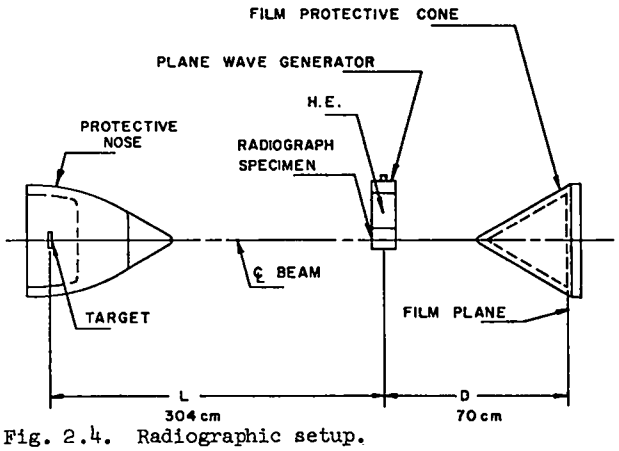

Fig. 2.4. Radiographic setup.

Although the procedure of comparing data on static radiographs with cathetometer measurements inherently eliminates problems of film shrinkage, shrinkage is measured and found to be about one part in 10^4, considerably less than our reading errors. Because the foils are all parallel, only one can be aligned simultaneously with the x-ray beam axis. Although it is possible to observe radiographically angular misalignments as small as 2 mrad, misalignment corrections are insignificant except for those foils farthest from the beam axis. The initial and final foil positions and their standard deviations are listed in Table 2-I for ten shots covering a range of 5 to 10 cm of run.

Detonation wave velocities are measured using a method developed by Hayes.[11] The arrival times of the detonation wave at accurately located discontinuities, such as the foils, are determined to within a few nanoseconds. The detonation wave velocity for each shot is found to be constant to within ±.025 mm/μsec and the velocity variation among shots is less than ±.040 mm/μsec. The detonation velocities and their standard deviations are listed in Table 2-II for nine shots. Each value represents the average velocity over the range in which the foil measurements are made. The mean detonation velocity (excluding the velocity for shot NW-432) is 7.886 ±.008 mm/μsec.

TABLE 2-I. FOIL POSITION DATA
(All distances in millimeters)

Shot NW-427

Foil No.	x_i	σ	x_f	σ
1	50.8743	0.0068	58.2258	0.2004
2	57.2262	0.0063	64.3882	0.1323
3	63.5705	0.0055	70.1641	0.0899
4	69.9226	0.0113	75.8652	0.0797
5	76.2629	0.0042	81.3592	0.1240
6	82.6105	0.0071	86.6121	0.0491
7	88.9395	0.0072	91.7140	0.0746
8	95.2769	0.0052	96.5462	0.0736
Det wave			100.8121	0.0722

Shot NW-428

Foil No.	x_i	σ	x_f	σ
1	50.8038	0.0095	57.4605	0.1955
2	57.1521	0.0080	63.2445	0.1160
3	63.4992	0.0093	69.1885	0.0730
4	69.8615	0.0122	74.7300	0.1064
5	76.2091	0.0079	79.9135	0.1207
6	82.5682	0.0105	84.9545	0.0720
7	88.9146	0.0084	89.7665	0.1077
Det wave			92.5010	0.0865

Shot NW-439

Foil No.	x_i	σ	x_f	σ
1	31.6977	0.0061	38.5099	0.1694
2	38.0382	0.0043	44.7809	0.1749
3	44.4033	0.0071	51.0221	0.1621
4	50.7542	0.0050	56.9119	0.1167
5	57.1103	0.0048	62.7889	0.1302
6	63.4248	0.0076	68.2060	0.0665
7	69.7632	0.0034	73.5548	0.0763
8	76.1141	0.0040	78.5865	0.0784
9	82.4673	0.0056	83.3569	0.1081
Det wave			86.3013	0.0947

Shot NW-430

Foil No.	x_i	σ	x_f	σ
1	25.3662	0.0084	31.7279	0.2056
2	31.7231	0.0069	38.1425	0.1061
3	38.0736	0.0064	44.2500	0.1137
4	44.4341	0.0076	50.3856	0.1205
5	50.8163	0.0063	56.3408	0.1183
6	57.1798	0.0063	61.9216	0.0923
7	63.5213	0.0044	67.2602	0.0878
8	69.8919	0.0061	72.3068	0.0599
9	76.2395	0.0058	77.1217	0.0540
Det wave			79.8317	0.0971

TABLE 2-I. FOIL POSITION DATA (Continued)
(All distances in millimeters)

Shot NW-431

Foil No.	x_i	σ	x_f	σ
1	19.0136	0.0039	24.7990	0.2115
2	25.3682	0.0055	31.0831	0.1948
3	31.6932	0.0055	37.4803	0.1984
4	38.0372	0.0044	43.5858	0.2252
5	44.3845	0.0053	49.5993	0.1485
6	50.7487	0.0064	54.8230	0.1087
7	57.1269	0.0080	60.6873	0.1205
8	63.4774	0.0072	65.8547	0.0925
9	69.8182	0.0071	70.6586	0.1009
Det wave			73.7193	0.0857

Shot NW-432

Foil No.	x_i	σ	x_f	σ
1	12.6797	0.0042	17.9611	0.1383
2	19.0323	0.0046	24.4520	0.1364
3	25.3795	0.0069	30.8801	0.1548
4	31.7359	0.0064	37.0148	0.0646
5	38.0643	0.0053	43.0183	0.0855
6	44.4247	0.0061	48.8425	0.0780
7	50.7889	0.0068	54.3893	0.0849
8	57.1510	0.0060	59.5665	0.0749
9	63.4927	0.0077	64.4993	0.0716
Det wave			66.0057	0.1545

This data set is omitted from the analysis on statistical grounds (see Appendix F).

Shot NW-442

Foil No.	x_i	σ	x_f	σ
1	6.3715	0.0043	10.9653	0.2245
2	12.7322	0.0039	17.2549	0.1874
3	19.0825	0.0048	23.8693	0.1716
4	25.4388	0.0038	30.2419	0.1801
5	31.7746	0.0055	36.2763	0.0996
6	38.1368	0.0045	42.1866	0.1015
7	44.4925	0.0049	47.7683	0.0857
8	50.8666	0.0058	52.9973	0.1191
9	57.2174	0.0049	57.9901	0.0861
Det wave			61.0199	0.0127

Shot NW-434

Foil No.	x_i	σ	x_f	σ
1	31.6563	0.0059	35.6361	0.0941
2	37.9622	0.0072	41.2667	0.0959
3	44.3197	0.0078	46.6358	0.0874
4	50.6708	0.0073	51.6324	0.0686
Det wave			54.6107	0.1120

Shot NW-433

Foil No.	x_i	σ	x_f	σ
1	6.3613	0.0057	10.5151	0.1982
2	12.7246	0.0041	16.8435	0.2031
3	19.0781	0.0062	23.4316	0.1848
4	25.4287	0.0072	29.6411	0.1514
5	31.7807	0.0092	35.6777	0.0860
6	38.0982	0.0113	41.3465	0.1599
7	44.4444	0.0082	46.8846	0.1022
8	50.8176	0.0105	51.9389	0.1226
Det wave			56.0128	0.0878

Shot NW-435

Foil No.	x_i	σ	x_f	σ
1	6.3390	0.0047	10.5488	0.1740
2	12.6702	0.0073	16.8452	0.1524
3	19.0352	0.0055	22.9796	0.0898
4	25.3692	0.0059	29.0733	0.1371
5	31.7302	0.0044	34.8788	0.0411
6	38.0553	0.0063	40.3304	0.0838
7	44.3939	0.0053	45.4155	0.1100
Det wave			48.3455	0.0918

TABLE 2-II. DETONATION WAVE VELOCITIES

Shot NW-	Foil Measurement Range (mm) Beginning	X	D (mm/μsec)
427	50.8743	100.8121	--[a]
428	50.8038	92.5010	7.9093 ±.0113
439	31.6977	86.3013	7.9137 ±.0021
430	25.3662	79.8317	7.8787 ±.0083
431	19.0136	73.7193	7.8889 ±.0128
432	12.6797	66.0057	7.8679 ±.0068
442	6.3715	61.0199	7.8971 ±.0047
433	6.3613	56.0128	7.8889 ±.0247
434	31.6563	54.6107	7.8661 ±.0102
435	6.3390	48.3455	7.8479 ±.0070

Mean Velocity (excluding the velocity for shot NW-432) = 7.8863 ±.0077

[a]The detonation wave velocity for this shot is omitted because of faulty electronics.

III. DATA ANALYSIS

A. Determination of the Flow from the One-Dimensional Euler Equations

The data listed in Table 2-I can be described by a function $x_f = x_f(x_i, X)$ in a given region of analyticity and the detonation velocity can be described by $D = D(X)$ (for most purposes we take D as constant at 7.886 mm/μsec). Given this information, then the density, particle velocity, pressure, and internal energy can be determined from the one-dimensional Euler equations. The density, ρ, is determined from the conservation of mass as

$$\rho(x_i, X) = \rho_o \left(\frac{\partial x_f}{\partial x_i}\right)_X^{-1} , \tag{3.1}$$

where ρ_o is the density of the unreacted explosive. Notice that the density can be calculated from the data of a single shot, whereas the calculation of any other flow variable requires data from several shots because time derivatives along particle paths are involved. The particle velocity, u, is given by

$$u(x_i, X) = D\left(\frac{\partial x_f}{\partial X}\right)_{x_i} . \tag{3.2}$$

The pressure, p, is determined from the conservation of momentum

$$\frac{\partial p}{\partial x_i} = -\rho_o D \frac{\partial u}{\partial X} , \tag{3.3}$$

and the internal energy, E, from the conservation of energy

$$\frac{\partial E}{\partial X} = p\rho^{-2} \frac{\partial \rho}{\partial X} . \tag{3.4}$$

The initial conditions for the integration of Eqs. (3.3) and (3.4) are obtained from the Rankine-Hugoniot equations as

$$\hat{p}(X) = \rho_o D \hat{u} , \tag{3.5}$$

$$\hat{E}(x_i) = E_o + \hat{u}^2/2 , \tag{3.6}$$

where $\hat{u} = u(x_i = X, X)$ and the pressure and particle velocity of the unreacted explosive are taken as zero.

The physical interpretation of $\hat{p}$ depends upon the resolution of the data. If the data are sufficient to resolve the reaction zone, $\hat{p}$ corresponds to the von Neumann "spike" pressure.[12,13] On the other hand, if the reaction zone is too thin to be resolved and instantaneous reaction is assumed, $\hat{p}$ corresponds to the detonation pressure. The physical interpretation of $\hat{E}$ is similar to the interpretation of $\hat{p}$.

If the explosive products are in chemical equilibrium, the isentropic sound speed, c, can be calculated as

$$c(x_i, X) = \left(\frac{\partial p}{\partial X}\right)_{x_i}^{\frac{1}{2}} \left(\frac{\partial \rho}{\partial X}\right)_{x_i}^{-\frac{1}{2}} . \tag{3.7}$$

The type of detonation (strong, Chapman-Jouguet, or weak) can, in general, be determined by comparing $(u + c)$ with D. However, if D is constant and we assume instantaneous reaction followed by a centered simple wave, then a Chapman-Jouguet detonation is automatically obtained if we attach the unsteady rarefaction to the detonation front. Moreover, a weak detonation is produced when a region of constant state is placed between the detonation front and the unsteady rarefaction. Strong detonations cannot exist under these assumptions; hence, the type of detonation (Chapman-Jouguet or weak) simply depends upon the range of data that are fitted with the unsteady rarefaction. Similar difficulties arise if we assume a steady reaction zone instead of instantaneous reaction.

To carry out the analysis, we must determine analytic expressions for $x_f(x_i, X)$ and $D(X)$. The classical theory of detonation provides the simplest

reasonable forms for x_f and D and is taken as the starting point.

B. Chapman-Jouguet/Taylor Wave Model

The classical theory of detonation consists of an instantaneous Chapman-Jouguet detonation followed by a centered simple wave (Taylor wave). The theory contains the following physical assumptions: (1) constant detonation velocity, (2) instantaneous reaction to a sonic state relative to the detonation front, and (3) self-similar flow following the detonation wave. Each of these assumptions, excluding the Chapman-Jouguet hypothesis, is checked with the data.

1. Test of the Physical Assumptions. As shown in Sec. II, the measured detonation velocity is constant within ±.025 mm/μsec in any one shot. Hence, we take D as constant and use the mean value of 7.886 mm/μsec to represent all the data. This mean value deviates less than ±.040 mm/μsec from the detonation velocity of any one shot.

With regard to the second assumption, neither the radiographs nor the plotted data show any indication of a finite reaction zone. The fact that the plotted data show no indication is not surprising, since the closest foil to the detonation front is about 2 mm behind it. Earlier measurements of reaction zone thickness[13] indicate that it is probably an order of magnitude smaller. Hence, for present purposes, we assume instantaneous reaction. With this assumption and the constancy of D, the sonic nature of the flow cannot be checked with only these data. Thus, we assume the Chapman-Jouguet hypothesis which attaches the Taylor wave to the detonation front. The possibility of a weak detonation is discussed in Sec. IV.

To check the assumption of (geometric) self-similarity, we plot y vs Y where

$$y = x_f/X \quad , \tag{3.8}$$

$$Y = x_i/X \quad , \tag{3.9}$$

and X is the distance of run associated with each shot. The y, Y values and their respective standard deviations are listed in Appendix A. The plotted values are shown in Fig. 3.1. The data points should lie along a single curve if the flow is geometrically similar. This is very nearly the case for most data points. For small values of Y, there is some spread in the data. This is to be expected,

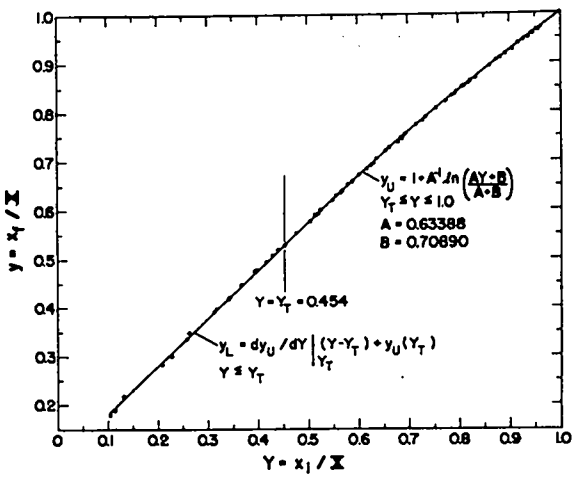

Fig. 3.1. Final foil position, x_f, vs initial foil position, x_i, both divided by the position, X, of the detonation front at the time of measurement of x_f. The points are the experimental data, the curve a fit.

however, because the flow in this region is governed primarily by the transmitted rarefaction from the P-081 driver, which is not a geometrically similar flow.

Since the data occupy two regions of analyticity, we cannot hope to describe all the data with a single analytic expression. The two regions are joined by a characteristic curve across which the first derivative of the flow variables has a finite jump. We denote this characteristic by Y_T and refer to it as the terminal characteristic of the Taylor wave. Within the Taylor wave region, the partial differential equations, Eqs. (3.1) to (3.7), are replaced by the following set or ordinary differential equations. Given y(Y) and D = constant we have

$$\rho(Y)/\rho_o = (y')^{-1} \quad , \tag{3.10}$$

$$c(Y)/D = Y(\rho/\rho_o)^{-1} \quad , \tag{3.11}$$

$$u(Y)/D = y - c/D \quad , \tag{3.12}$$

$$p'(Y)/\rho_o D^2 = (c/D)^2(\rho/\rho_o)' \quad , \tag{3.13}$$

$$\gamma = c^2\rho/p \quad , \tag{3.14}$$

$$E'(Y)/D^2 = (p/\rho_o D^2)(\rho/\rho_o)^{-2}(\rho/\rho_o)' \quad , \tag{3.15}$$

where the constants of integration are

$$\hat{p}/\rho_o D^2 = \hat{u}/D \quad , \tag{3.16}$$

$$\hat{E}/D^2 = E_o/D^2 + (\hat{u}/D)^2/2 \quad . \qquad (3.17)$$

Here, (^) means a quantity evaluated at Y = 1 (the Chapman-Jouguet point).

In the region following the Taylor wave, the flow is most probably influenced by the transmitted rarefaction from the P-081 driver. However, there is only a slight spread in the data and, moreover, the data lie very nearly along a straight line. Hence, for computational ease, we approximate this region by a constant state. The effect of this approximation on the determination of Y_T and hence the calculated flow in the Taylor wave is discussed below.

2. Location of the Terminal Characteristic of the Taylor Wave. The terminal characteristic, Y_T, of the Taylor wave is located by trial and error. We guess a value of Y_T and fit the data in the Taylor wave region with some form

$$y_U = y(Y \; ; \; a_n) \qquad (3.18)$$

while the data in the trailing constant state are fitted with

$$y_L = b_1 Y + b_2 \quad , \qquad (3.19)$$

where a_n and b_n are adjustable parameters. We seek to match the density at the end of the Taylor wave, calculated from Eq. (3.10), with the density in the constant state, which is simply ρ_o/b_1.

A preliminary investigation of fitting forms, y_U, indicates that only two parameters are needed to describe the data accurately (see Appendix B). In an effort to remove fitting form bias in the calculation of Y_T, nine fitting forms are used (each fits the data equally well) and the mean density at the end of the Taylor wave is compared with the density in the constant state. Each of the nine fitting forms is chosen a priori to pass through the point Y = 1, y = 1. This is done because the unreacted explosive is stationary ($u_o = 0$). A curve passing above the point 1,1 indicates forward motion of the unreacted explosive whereas a curve passing below indicates backward motion. The results for three guesses at Y_T are given in Table 3-I. The fitting form numbers refer to equations in Appendix B.

The value $Y_T = 0.454$ is selected as the terminal characteristic. To obtain continuity of y and ρ at Y_T, we select fitting form (B7a) (see Sec. 3 below) which is representative of the mean and require

$$y_L = y_U' \Big|_{Y_T} (Y - Y_T) + y_U \Big|_{Y_T} \quad . \qquad (3.20)$$

This changes b_1 from 1.0017 to 1.0033 and b_2 from 0.078036 to 0.074254 and increases the standard deviation of the fit, defined in Eq. (3.28), in the constant state from 0.0038 to 0.0049. For comparison, the standard deviations of the data points in the constant state range from 0.0015 to 0.0037 (see Appendix A).

It is found after the fact that the location of the terminal characteristic has very little effect upon the calculation of the flow in the Taylor wave. The mean Chapman-Jouguet pressure, for example, varies by less than 3 kbar for Y_T between 0.430 and 0.515. Consequently, the accuracy of the constant state approximation to the transmitted rarefaction from the driver is unimportant for this purpose.

3. Calculation of the Complete Flow. Fitting form (B7a) has the form

$$y_U = 1 + A^{-1} \ln\left(\frac{AY + B}{A + B}\right) \quad , \qquad (3.21)$$

where A = 0.63388 and B = 0.70890. The implied flow calculated from Eqs. (3.10) to (3.17) is

TABLE 3-I. COMPARISON OF THE COMPRESSION (ρ/ρ_o) AT THE END OF THE TAYLOR WAVE WITH THE COMPRESSION IN THE TRAILING CONSTANT STATE.

The compression at the end of the Taylor wave is calculated from Eq. (3.10) for the fitting forms given by Eqs. (B1a) to (B8a) and (B9). The compression in the constant state is calculated from a linear fit to the remaining data.

Fitting Form	Position of the Terminal Characteristic, Y_T = 0.5046	0.4769	0.4540
	Compression ρ/ρ_o		
B1a	1.0282	1.0150	0.9991
B2a	1.0095	0.9936	0.9737
B3a	1.0334	1.0185	1.0042
B4a	1.0516	1.0398	1.0281
B5a	1.0038	0.9871	0.9659
B6a	1.0149	1.0006	0.9821
B7a (ref.)	1.0272	1.0122	0.9967
B8a	1.0356	1.0221	1.0079
B9	1.0433	1.0309	1.0179
Mean	1.0275 ±.0052	1.0133 ±.0057	0.9973 ±.0068
Linear Fit	1.0030 ±.0072	0.9993 ±.0075	0.9983 ±.0082

$$\rho/\rho_o = AY + B \quad , \tag{3.22}$$

$$c/D = Y(\rho_o/\rho) \quad , \tag{3.23}$$

$$u/D = y_U - c/D \quad , \tag{3.24}$$

$$p/\rho_o D^2 = 1 - A^{-2}\left[\rho(1 - \rho_o B/\rho)^2 + 2(\hat{\rho} - \rho)\right]/\rho_o + 2BA^{-2}\,\ell n\,(\hat{\rho}/\rho) \quad , \tag{3.25}$$

$$\gamma = c^2\rho/p \quad , \tag{3.26}$$

$$(E - E_o)/D^2 = (\hat{u}/2D)^2 + (\rho - \hat{\rho})(\rho_o/\hat{\rho} - 2A^{-2})/\rho + (B/2A)^2\,(\hat{\rho}^2 - \rho^2)/\rho\hat{\rho} + A^{-2}\,(1 + 2B\rho_o/\rho)\,\ell n\,(\rho/\hat{\rho}) \quad . \tag{3.27}$$

The flow in the Taylor wave region ($Y \geq 0.454$) is calculated from Eq. (3.21) and the flow behind the Taylor wave is calculated from Eq. (3.20). An x,t plot of the calculated flow with the data superimposed is shown in Fig. 3.2. The detonation front, tail characteristic of the Taylor wave, and the piston path are shown. The calculated particle paths are shown as solid lines in the Taylor wave region and as dashed lines in the region of constant state. In the Taylor wave region, the agreement appears to be very good. The approximation of the transmitted rarefaction from the P-081 driver by a constant state appears to do quite well. Figures showing $y(Y)$, $\Delta y(Y)$, $u(Y)/D$, $c(Y)/D$, $\rho(Y)/\rho_o$, $p(Y)/\rho_o D^2$, $p(Y)$ in megabars, $(E(Y)-E_o)/D^2$, $\gamma(Y)$, $u(y)/D$, $c(y)/D$, $\rho(y)/\rho_o$, $p(y)/\rho_o D^2$, $\ell n\,(p/\rho_o D^2)$ vs $\ell n\,(\rho/\rho_o)$, $p(\rho/\rho_o)/\rho_o D^2$, $\gamma(\rho/\rho_o)$, and a typical

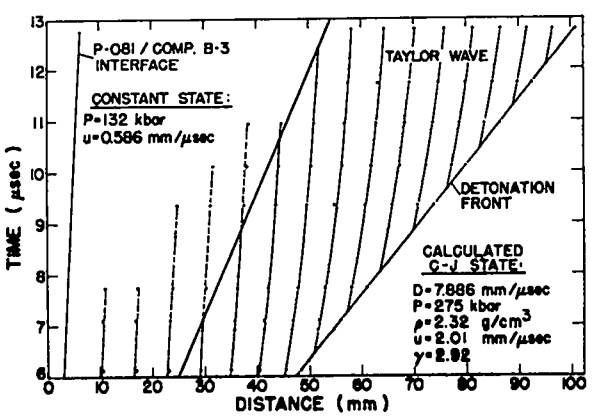

Fig. 3.2. Calculated particle paths with the data points superimposed. The calculated curves and values come from a two-parameter fit to the data [(Eq. (3.21)].

negative characteristic are contained in Appendix D together with the tabulated values.

4. Error Analysis. An appropriate quantity to compare with the standard deviations of the data points listed in Appendix A is the standard deviation of the fit

$$SDF(n,N) = \left[\frac{1}{(n-N)}\sum_{1}^{n}(\Delta y)^2\right]^{\frac{1}{2}} \quad , \tag{3.28}$$

where n is the number of data points being fitted, N is the number of adjustable parameters in the fitting form, and Δy is the difference between the data and calculated values. In the Taylor wave region, $SDF(53,2) = 0.0017$ when $Y_T = 0.454$ and we use fitting form (B7a) [Eq. (3.21)]. The standard deviations of the data points in the Taylor wave region range from 0.0008 to 0.0031.

The standard deviations of the flow variables are calculated from the standard deviations of the parameters, $\sigma(A)$ and $\sigma(B)$, and the standard deviation of the mean detonation velocity, $\sigma(D)$. The details of the calculation are given in Appendix E. In estimating the total standard deviation of any flow variable, we also include the standard deviation of the mean for the 11 different fitting forms, Eqs. (B1a to B8a), (B9), (B10), and (B11), listed in Appendix B. In Table 3-II we list the components of the total standard deviation of each flow variable as

1. σ_{AB}, standard deviation arising from $\sigma(A)$ and $\sigma(B)$ alone,
2. σ_D, standard deviation arising from $\sigma(D)$ alone,
3. σ_{ff}, standard deviation of the mean for eleven fitting forms, and
4. σ, total standard deviation.

The values are listed at the detonation front and at the end of the Taylor wave, because the errors are largest at these extremes. The total standard deviation is obtained by combining the component errors as independent, i.e.,

$$\sigma = (\sigma_{AB}^2 + \sigma_D^2 + \sigma_{ff}^2)^{\frac{1}{2}} \quad .$$

We are unable to arrive at any useful estimate of the systematic errors.

5. Comparison with Other Work. Several flow variables calculated for various calibrated isentropes (γ-law, BKW-HOM, and JWL) using the classical

TABLE 3-II. FLOW VARIABLES

Calculated with the classical model using Eq. (3.21) and their estimated standard deviations at the detonation front and the end of the Taylor wave.

Flow Variable	Value	Standard Deviation σ_{AB}	σ_D	σ_{ff}	σ
$\hat{\rho}$	2.32 g/cm^3	0.010	--	0.007	0.012
$\hat{c}$	5.87 mm/μsec	0.024	0.006	0.017	0.030
$\hat{u}$	2.01 mm/μsec	0.024	0.002	0.017	0.029
$\hat{p}$	275 kbar	3.2	0.6	2.3	4.0
$\hat{\gamma}$	2.92	0.043	--	0.032	0.054
$\rho(\gamma_T)$	1.72 g/cm^3	0.009	--	0.011	0.014
$c(\gamma_T)$	3.59 mm/μsec	0.018	0.003	0.024	0.030
$u(\gamma_T)$	0.586 mm/μsec	0.024	0.001	0.026	0.035
$p(\gamma_T)$	132 kbar	1.8	0.3	1.8	2.5
$\gamma(\gamma_T)$	1.69	0.029	--	0.035	0.046

Chapman-Jouguet detonation model with a constant velocity driver-Composition B-3 interface as described above are compared with the corresponding variables calculated in this work. The form of each isentrope is as follows:

γ-law isentrope:[7]

$$p = \hat{p}(\rho/\hat{\rho})^{\gamma} \quad , \quad \hat{p} = \rho_o D^2/(\gamma+1) \quad ,$$
$$\hat{\rho} = \rho_o(\gamma+1)/\gamma \quad , \qquad (3.29)$$

BKW-HOM isentrope:[8]

$$\ell n\, p = a_1 + a_2 \ell n\, v + a_3 (\ell n\, v)^2 + a_4 (\ell n\, v)^3 + a_5 (\ell n\, v)^4 \quad ,$$
$$v = 1/\rho \quad , \qquad (3.30)$$

JWL isentrope:[9]

$$p = a_1 V^{a_2} + a_3 e^{a_4 V} + a_5 e^{a_6 V} \quad ,$$
$$V = \rho_o/\rho \quad . \qquad (3.31)$$

For uniformity, we adjust the Chapman-Jouguet pressure, $\hat{p}$, for each isentrope to be 0.292 Mbar when D = 0.7886 cm/μsec and ρ_o = 1.730 g/cm^3. This value of Chapman-Jouguet pressure has been measured by Deal[14] for Composition B having an RDX/TNT content of 64/36 wt % and an initial density of 1.713 g/cm^3. The correction of this value to our Composition B-3 is negligible. For the γ-law isentrope, this implies γ = 2.6848. For the BKW-HOM and JWL isentropes, we adjust two parameters in each to satisfy the following relations which hold at the Chapman-Jouguet point.

$$\hat{p}(\hat{v} \; ; \; a_n) = \rho_o D^2(1 - \hat{v}\rho_o) \quad , \qquad (3.32)$$

$$\frac{\partial p}{\partial v}(\hat{v} \; ; \; a_n) = -\rho_o D^2 \quad . \qquad (3.33)$$

Given $\hat{p}$ = 0.292 Mbar and $\hat{v} = (1 - \hat{p}/\rho_o D^2)/\rho_o$, we solve Eqs. (3.32) and (3.33) for a_1 and a_2 in the case of BKW-HOM and for a_1 and a_3 in the case of JWL. Equations (3.32) and (3.33) are identically satisfied by the γ-law isentrope as given by Eq. (3.29).

The calibrated parameters for the three isentropes are listed in Table 3-III. These parameters, we believe, represent the most current values. For each isentrope, the standard deviation of the fit is also given for comparison with the value 0.0017 obtained with Eq. (3.21). The quantities in parentheses result from a least-squares fit to the data. By allowing two free parameters in the BKW-HOM (a_2, a_3) and JWL (a_3, a_4) forms, we can accurately describe the data; thus, neither form is preferable in this regard. In fact, in Appendix B these forms are shown to be statistically equivalent to nine other two-parameter forms. The third parameter (a_1

TABLE 3-III. PARAMETER VALUES FOR THE γ-LAW, BKW-HOM, AND JWL ISENTROPES.

Parameter	Isentrope γ-Law	BKW-HOM	JWL
γ	2.6848 (2.5980)	--	--
a_1	--	-3.4160 (-2.4892)	0.012095 (0.092815)
a_2	--	-2.3316 (0.26037)	-1.34
a_3	--	0.25961 (2.0275)	5.0996 (43.074)
a_4	--	0.028355	-4.2 (-8.1024)
a_5	--	-0.012436	0.076783
a_6	--	--	-1.1
SDF(53,0)	0.0039	0.0034	0.0076
SDF(53,1)	(0.0036)	--	--
SDF(53,2)	--	(0.0018)	(0.0018)

Parameter values correspond to p(Mbars) and v(cm^3/g). The values in parentheses correspond to a fit to the data.

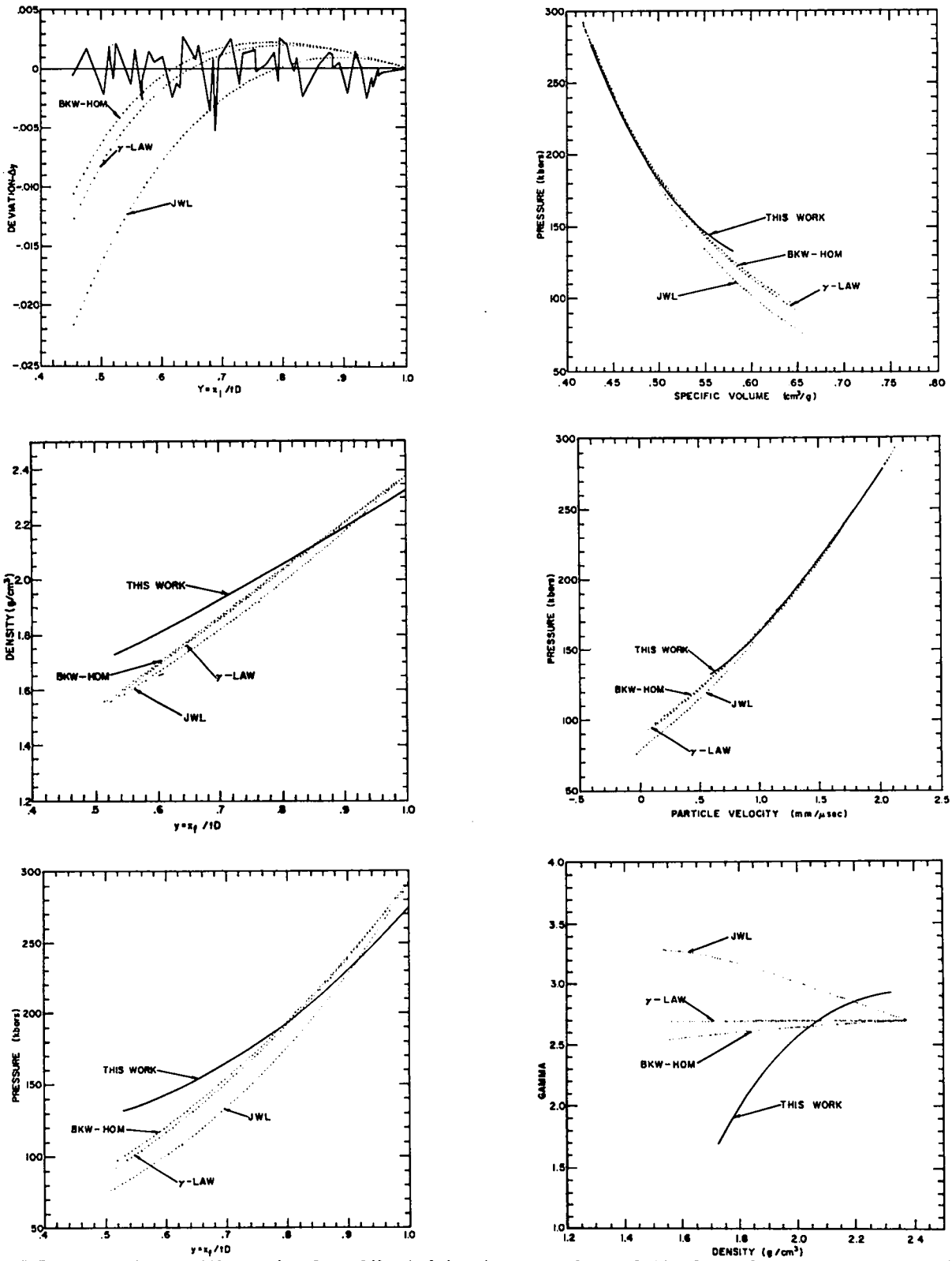

Fig. 3.3. Comparisons with previously calibrated isentropes. The analytic form of each isentrope is given in Eqs. (3.29 to 3.31) and the parameter values are listed in Table 3-III. The first figure shows differences in values of y relative to values calculated with Eq. (3.21). The sawtooth curve is the difference between the data points and Eq. (3.21).

in each case) that changes is dependent upon the two free parameters and is determined along with the value of $\hat{v}$ by simultaneous solution of Eqs. (3.32) and (3.33). Although the single-parameter γ-law form does remarkably well, it is clear that a single parameter does not provide an accurate description of the data.

The upper left-hand frame of Fig. 3.3 shows four curves which represent differences in y relative to the values calculated with Eq. (3.21). The sawtooth curve represents differences with the actual data points. The three dotted curves represent differences between the calibrated isentropes and Eq. (3.21). Toward the end of the Taylor wave, all the calibrated isentropes yield values of y considerably below the data points. In the remaining five frames we show comparisions of $\rho(y)$, $p(y)$, $p(v)$, $p(u)$, and $\gamma(\rho)$ calculated from the calibrated isentropes and Eq. (3.21).

IV. DISCUSSION OF RESULTS

The results obtained from the analysis of the embedded foil data are summarized in Table 4-I. The Chapman-Jouguet pressure of 275 ±4 kbar has been compared with other values obtained by different measurement techniques (see Ref. 16). Values ranging from ≤ 268 ±6 to 312 ±5 kbar are cited. The lowest value is obtained with a new x-ray technique,[16] and the higher values (292 and 312) are inferred from measurements of the free surface velocity of driven inert plates. No satisfactory explanation for the large range of values is presented and there appears to be no reason to choose one value as "correct" in preference to the others.

The results presented in Table 4-I have been obtained within the context of the classical model of detonation. It is important to realize, however, that other models which involve different physical assumptions exist and describe the data equally well. Moreover, the results obtained are generally different than those reported for the classical model, although, in the two alternate models we consider below, the differences are not statistically significant.

Observations of gas detonations show[17,18] that the flow immediately behind the front, while not one-dimensional in the small, is on the average supersonic with Mach number 1.10 to 1.15. Furthermore, mechanisms for steady reaction zone solutions which terminate in a weak state have been described.[19,20] Hence, a weak detonation with instantaneous reaction and a trailing self-similar flow is investigated as an alternate model for the data. A weak detonation is produced if we separate the rarefaction wave from the detonation front by a small region of constant state. The detonation Mach number, M, is related to the size of the constant state region, δy, by

$$M = 1 + D\delta y/\hat{c} \quad . \tag{4.1}$$

Here, $\hat{c}$ is the acoustic velocity in the constant state. Mach numbers ranging from 1.0 (Chapman-Jouguet detonation) to 1.15 are investigated. The results are given in Table 4-II. For Mach number 1.03, the density at the front is decreased by 1% and the pressure by 3% of the Chapman-Jouguet values and the SDF (52,2) increases by 0.03%. The constant state region which has $\delta y = 0.02$ contains no foils. For Mach number 1.15, the density and pressure are decreased by 4% and 12%, respectively, and the SDF (52,2) is increased by 13%. In this case, the constant state region has $\delta y = 0.10$ and contains 13 foils. We conclude that the data are also well described by a weak detonation with Mach number a few percent greater than unity. However, it is unlikely that we have a Mach number as large as 1.15.

We turn our attention now to the possibility of a slightly time-dependent detonation as another possible model for the data. Slight time dependence would not be detectable in the plot of y vs Y (Fig. 3.1), because the data sets are not distinguished. To investigate this question, we make use of the fact that the density can be calculated from the data of a single shot using only conservation of mass, Eq. (3.1). Also, the pressure at the front can be calculated from the density using the Rankine-Hugoniot equations if we assume instantaneous reaction.

For each shot we fit the data points that lie in the range $0.454 \le x_i/X \le 1$ with the form

$$x_f = X + XA^{-1} \ln\left(\frac{Ax_i/X + B}{A + B}\right) \quad . \tag{4.2}$$

This fitting form, although equivalent to Eq. (3.21), does not invoke the assumption of self-similar flow because the values of A and B are free to change from one shot to the next. The values of A, B, $\hat{\rho}$,

TABLE 4-I. SUMMARY OF RESULTS OBTAINED FOR COMPOSITION B-3 (60% RDX, 40% TNT, $\rho_o = 1.730$ g/cm^3).

Fit:	$y = x_f/X$, $Y = x_i/X$, $X = Dt$,
	$y = 1 + A^{-1} \ln\left(\frac{AY+B}{A+B}\right)$, $A = 0.63388 \pm .020$, $B = 0.70890 \pm .015$
	$D = 7.886 \pm .008$ mm/μsec .
Calculated Flow:	$\rho/\rho_o = AY + B$, $c/D = Y\rho_o/\rho$, $u/D = y - c/D$
	$p/\rho_o D^2 = 1 - A^{-2}[(\rho/\rho_o)(1-\rho_o B/\rho)^2 + 2(\hat{p}-p)/\rho_o] + 2BA^{-2} \ln(\hat{\rho}/\rho)$,
	$\gamma = c^2\rho/p$
Chapman-Jouguet State:	$\hat{\rho} = 2.32 \pm .01$ g/cm^3 , $\hat{c} = 5.87 \pm .03$ mm/μsec ,
	$\hat{u} = 2.01 \pm .03$ mm/μsec , $\hat{p} = 275 \pm 4$ kbar, $\hat{\gamma} = 2.92 \pm .05$
Constant State:	$\rho = 1.72 \pm .01$ g/cm^3 , $c = 3.59 \pm .03$ mm/μsec
	$u = 0.586 \pm .04$ mm/μsec , $p = 132 \pm 3$ kbar , $\gamma = 1.69 \pm .05$

TABLE 4-II. DENSITY, PRESSURE, AND PERCENTAGE INCREASE IN THE STANDARD DEVIATION OF THE FIT FOR INCREASING VALUES OF THE MACH NUMBER.

The data in the rarefaction wave, $0.554 \le y \le 1 - \delta y$, are fitted with $y = (Y^B - 1)/AB + 1$. The data in the constant state, $1 - \delta y \le y \le 1$ are fitted by a linear extension through the point 1,1.

M	δy	$\hat{\rho}$(g/cm^3)	$\hat{p}$(kbar)	% Increase in SDF(52,2)
1.00	0.00	2.308	269.4	--
1.01	0.01	2.296	265.3	0.005
1.03	0.02	2.285	261.5	0.034
1.15	0.10	2.219	237.1	13.148

and $\hat{p}$ obtained for each shot are listed in Table 4-III. In Fig. 4.1, $\hat{\rho}$ and $\hat{p}$ are plotted as functions of the distance of run. The constant values obtained with the classical model, Eq. (3.21), are shown for reference. A linear fit to $\hat{\rho}(X)$ and $\hat{p}(X)$ reveals a slight upward trend. The density increases from 2.306 to 2.340 g/cm^3 and the pressure increases from 267.4 to 281.9 kbar.

In view of this, a slightly time-dependent detonation model is considered. This model which assumes only instantaneous reaction (the Chapman-Jouguet hypothesis and self-similar flow are not assumed) is also found to provide an accurate description of the data. The data are fitted with $x_f(x_i, X)$ given by

$$x_f = \frac{X}{1-B}\left[A\left(\frac{x_i}{X}\right)^B + (1 - A - B)\left(\frac{x_i}{X}\right)\right] , \quad (4.3)$$

where

$$A = a_1 X + a_2 , \quad (4.4)$$

$$B = a_3 X + a_4 . \quad (4.5)$$

This fitting form, which has two independent variables (x_i, X) and four parameters (a_1 through a_4), is analytically equivalent to Eq. (B3a) when A and B are constants. The standard deviation of the fit, SDF(53,4), is actually 1.4% larger than SDF(53,2) obtained with Eq. (B3a). (The reduction of 2 in the degrees of freedom has offset the slight reduction in the sum of the squares of the deviations.) The parameter values obtained from the least-squares fit are

$$a_1 = 0.20393 \times 10^{-3} \pm .189 \times 10^{-3} , \quad (4.6a)$$

$$a_2 = 0.24378 \pm .016 , \quad (4.6b)$$

$$a_3 = 0.43413 \times 10^{-2} \pm .302 \times 10^{-2} , \quad (4.6c)$$

$$a_4 = 1.1917 \pm .252 . \quad (4.6d)$$

The flow is calculated from Eqs. (3.1) to (3.6) using Eqs. (4.3) to (4.6) with D = 7.886 mm/μsec (strictly speaking, D must be increasing very slightly, about 0.1%, but this would have a negligible effect on the calculation). The results show

TABLE 4-III. PARAMETERS A AND B, DENSITY, AND PRESSURE AT THE DETONATION FRONT OBTAINED BY FITTING EACH DATA SET INDIVIDUALLY WITH EQ. (4.2) OVER THE RANGE $0.454 \le x_i/X \le 1$.

Shot NW-	Data Points Fit	X	A	B	$\hat{\rho}$(g/cm³)	$\hat{p}$(kbar)
427	8	100.8121	0.64602	0.69423	2.319	273.2
428	7	92.5010	0.72794	0.63131	2.352	286.0
439	7	86.3013	0.67309	0.68397	2.348	285.1
430	7	79.8317	0.70617	0.66111	2.365	288.5
431	6	73.7193	0.55019	0.77232	2.288	262.6
442	5	61.0199	0.53676	0.77974	2.278	259.4
433	5	56.0128	0.54198	0.77151	2.272	256.8
434	4	54.6107	0.64109	0.70812	2.334	277.1
435	4	48.3455	0.65280	0.70025	2.341	278.0
Classical Model:			0.63388	0.70890	2.323	74.7

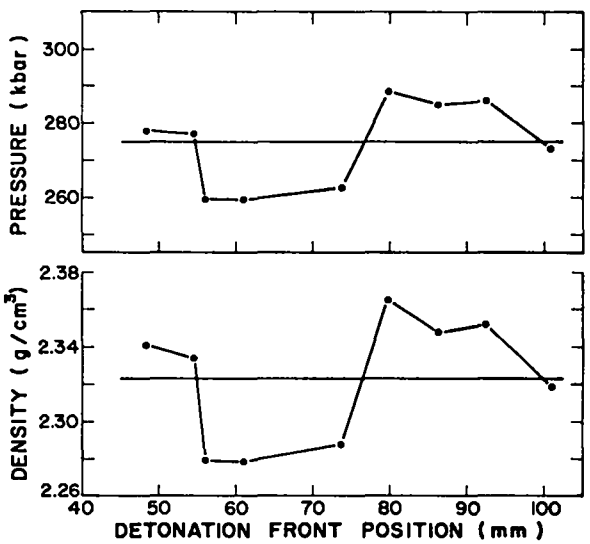

Fig. 4.1. Density and pressure at the detonation front calculated by fitting the foil data for individual shots with Eq. (4.2).

that the detonation pressure increases by about 12 kbar over the 52 mm of run. The average pressure is the same as the Chapman-Jouguet pressure (278.5 kbar) calculated from Eq. (B3a) with A and B constant.

Statistically, this slight increase is not significantly different than zero. Recall that the Chapman-Jouguet pressure varied from 267 to 291 kbar for the classical model when different fitting forms were used (see Appendix B). Furthermore, in the neighborhood of the Chapman-Jouguet point on any reasonable Hugoniot curve this pressure rise of 12 kbar could result from a very slight, about 0.1%, increase in D, which is well within its measurement error.

If we pursue this model further, to the point of calculating the detonation Mach number, we find a Mach number 1.03 at 48 cm of run which increases to 1.05 at 100 mm. This increasing Mach number indicates that the detonation is getting weaker as it propagates, whereas the increasing front pressure indicates the opposite. This contradiction may indicate a failure of our assumption of instantaneous reaction. However, it may be possible to remove the contradiction (i.e., obtain a decreasing Mach number) through a constrained least-squares fit. The Mach number will decrease if we require the parameters to satisfy the inequality

$$\frac{d\hat{u}}{dX} > \frac{dD}{dX} - M\frac{d\hat{c}}{dX} \quad , \tag{4.7}$$

where

$$\hat{u}(X) = D\frac{\partial x_f}{\partial X} \quad , \tag{4.8}$$

$$\hat{c}(X) = \frac{\rho_o}{\rho}\left[-D^2 - 2D^2\frac{\partial^2 x_f}{\partial X^2}\left(\frac{\partial^2 x_f}{\partial X \partial x_i}\right)^{-1} - 3\hat{u}\frac{dD}{dX}\left(\frac{\partial^2 x_f}{\partial X \partial x_i}\right)^{-1}\right]^{\frac{1}{2}} \quad . \tag{4.9}$$

The partial derivatives are evaluated at $x_i = X$. This constrained fit has not been attempted.

Mader[15] has performed a calculation with still a different model. Mader considered a system of 10.2 cm of Baratol (p_{CJ} = 137 kbar, D = 4.87 mm/μsec, ρ_o = 2.60 g/cm³) and 10.2 cm of Composition B-3 (p_{CJ} = 300 kbar, D = 7.98 mm/μsec, ρ_o = 1.73 g/cm³). In his time-dependent calculation with the BKW-HOM equation of state, the Baratol-Composition B-3 interface decelerates from an initial velocity of about 0.90 mm/μsec down to about 0.01 mm/μsec while the detonation wave travels 10 cm. The result of this interface motion is to place the end of the Taylor wave at about Y = 0.62 with non-self-similar flow for Y < 0.62. This implies that the data points for Y < 0.62 should occupy an area in the Y,y plane

(recall Fig. 3.1). This does not appear to be the case. However, the calculation indicates that the area would be very narrow. The maximum half-width would be about 0.004 measured normal to the curve shown in Fig. 3.1 and would occur at about Y = 0.25. Most probably, such a narrow region could not be statistically distinguished from a curve because the standard deviations in the data are nearly this size for many points.

In the course of the experimental work described herein, an x,t measurement of the P-081/Composition B-3 interface was made. The measurement indicates that the interface velocity is nearly constant at 0.52 mm/μsec over the range from 2 to 8 cm of run of the detonation front. Without reference to this result, we obtained from the foil data analysis a constant state with velocity of 0.59 mm/μsec and pressure of 132 kbar adjacent to the interface. This state implies the impact pressure from the P-081 driver is about 103 kbar, which is about 35 kbar lower than the detonation pressure for a slab of Baratol. The impact pressure for the P-081 may very well be less than its detonation pressure because of the inherent multidimensional effects known to be present in the P-081. A quantitative study of the P-081 is planned using the embedded foil technique.

As the final topic we consider the following question. What systematic displacement of the final foil positions would be sufficient to produce a Chapman-Jouguet pressure of 312 kbar (the largest experimental value reported in Ref. 16)? To investigate this question we take the fitting form given by Eq. (B3a), i.e.,

$$u/D = a_1 Y^{a_2} ,$$

and fix a_1 so as to yield the desired pressure of 312 kbar at Y = 1. The data are then fitted with parameter a_2 adjustable. The differences between the present data points and the calculated curve which represents the required systematic displacements are shown in Fig. 4.2. In general, the foils at the beginning of the Taylor wave would have to be moved forward and the foils near the end of the Taylor wave would have to be moved backwards. This would imply a density higher than we calculate with the classical model in the front and lower in the rear. For a detonation wave that has traveled

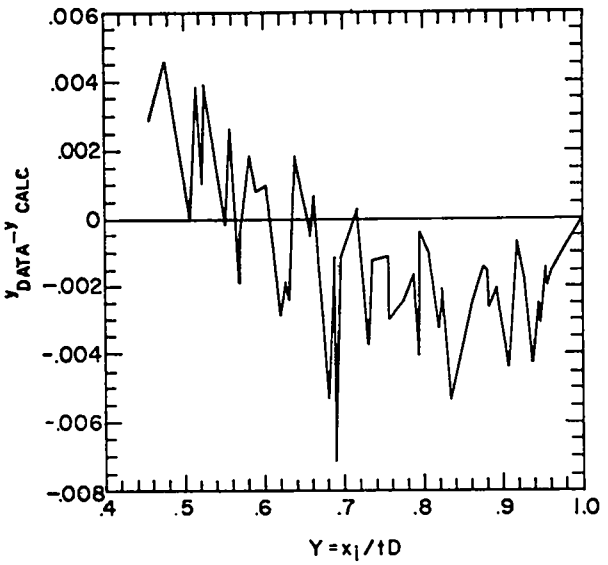

Fig. 4.2. Systematic displacement of final foil positions which is sufficient to produce a Chapman-Jouguet pressure of 312 kbar.

100 mm, the largest forward displacement would be about 0.3 mm and the largest backward displacement about 0.35 mm. These displacements are two to three times as large as the standard deviation of the measurements.

V. CONCLUSIONS

The initial and final foil positions recorded at nine discrete positions of the detonation front ranging from 48 to 101 mm are shown to scale with the detonation front position for a considerable distance (about 50% of the distance of run) behind the front . The detonation wave velocity is found to be 7.886 ±.008 mm/μsec over the range of interest and the "reaction zone" appears to be very thin. The data are accurately described within the context of the classical Chapman-Jouguet/Taylor wave model. The results of analyses show that the Chapman-Jouguet state for Composition B-3 (60% RDX, 40% TNT, initial density 1.730 g/cm^3) is described by: $\hat{p}$ = 275 ±4 kbar, $\hat{\rho}$ = 2.32 ±.01 g/cm^3, $\hat{u}$ = 2.01 ±.03 mm/μsec, and $\hat{\gamma}$ = 2.92 ±.05. The flow following the Taylor wave is found to be very nearly a constant state described by: p = 132 ±3 kbar, ρ = 1.72 ±.01 g/cm^3, u = 0.586 ±.04 mm/μsec, and γ = 1.69 ±.05.

The data can also be described, equally well, by a weak detonation with Mach number a few percent greater than unity. For a Mach number 1.03, the detonation pressure is about 97% of the Chapman-

Jouguet value. A slightly time-dependent detonation can also be used to describe the data. With this model, the detonation pressure is found to increase by 12 kbar over the range from 48 to 101 mm. The mean pressure is the Chapman-Jouguet value. Neither of these models yields results that are statistically different than those obtained with the classical model.

When the flow is calculated from various calibrated isentropes (γ-law,[7] BKW-HOM,[8] and JWL[9]) using the classical model with a constant velocity driver-Composition B-3 interface, none of the isentropes accurately describes the initial and final position data. The standard deviations of the data points range from 0.0008 to 0.0031, whereas the standard deviation of the fit with the calibrated isentropes is 0.0039, 0.0034, and 0.0076, respectively. For comparison, the two-parameter least-squares fit with Eq. (3.21) gives 0.0017. If two parameters are adjusted in either the BKW-HOM or the JWL form, then they describe the data as well as does Eq. (3.21). Thus, neither form is preferable for fitting the data.

In assessing any of these results, we must bear in mind that the effects of the foils are not fully known at present. Measurement of the detonation velocity on a system identical to that used here but without foils gives a velocity of 7.915 mm/μsec, which is 0.4% higher than the velocity of 7.886 mm/μsec measured with foils. Reference 16 describes experiments which compare the free surface velocities of driven plates for explosive systems with and without foils. The free surface velocity is found to be 3.60 mm/μsec with foils and 3.66 mm/μsec without foils. The inferred Chapman-Jouguet pressures are 312 ±5 and 317 ±8 kbar, respectively. It is concluded that the foils do not seriously affect the velocity of a driven plate.[16] Further experiments are planned to compare both the density distribution and the detonation state with and without foils.

VI. ACKNOWLEDGMENTS

The authors thank W. C. Davis and Wildon Fickett for their valuable suggestions and stimulating discussions and R. K. London for making the experimental assemblies and reading the radiographs.

APPENDIX A. CALCULATED VALUES OF Y, y, AND ASSOCIATED STANDARD DEVIATIONS

The values of Y and y are calculated from Eqs. (3.8) and (3.9). The standard deviations in Y and y are calculated as

$$\sigma(Y) = X^{-1}\left[\sigma(x_i)^2 + Y^2\,\sigma(X)^2\right]^{\frac{1}{2}} , \qquad (A1)$$

$$\sigma(y) = X^{-1}\left[\sigma(x_f)^2 + y^2\,\sigma(X)^2\right]^{\frac{1}{2}} , \qquad (A2)$$

respectively, where $\sigma(x_i)$, $\sigma(x_f)$, and $\sigma(X)$ are the standard deviations in x_i, x_f, and X, respectively, as listed in Table 2-I. Equations (A1) and (A2) assume that x_i, X and x_f, X, respectively, are stochastically independent variables so that the associated covariances vanish. The values of Y, y, and the associated standard deviations are designated as YI, YF, and STD. DEV., respectively, in the following listings.

YI,YF VALUES AND STANDARD DEVIATIONS FOR DATA SET NW-427

YI	STD. DEV.	YF	STD. DEV.
.50464478	.00036766	.57756757	.00203044
.56765210	.00041132	.63869516	.00138978
.63058403	.00045490	.69598887	.00102161
.69359333	.00050923	.75254062	.00095681
.75648558	.00054338	.80703804	.00135904
.81945024	.00059109	.85914389	.00078474
.88223041	.00063586	.90975190	.00098595
.94509389	.00067882	.95768464	.00100171
DETONATION FRONT		1.00000000	.00101284

YI,YF VALUES AND STANDARD DEVIATIONS FOR DATA SET NW-428

YI	STD. DEV.	YF	STD. DEV.
.54922433	.00052376	.62118788	.00219187
.61785386	.00058421	.68371693	.00140762
.68647042	.00064976	.74797570	.00105453
.75525129	.00071846	.80788316	.00137617
.82387326	.00077514	.86392039	.00153470
.89261954	.00084239	.91841710	.00115908
.96122853	.00090344	.97043816	.00147619
DETONATION FRONT		1.00000000	.00132247

YI,YF VALUES AND STANDARD DEVIATIONS FOR DATA SET NW-439

YI	STD. DEV.	YF	STD. DEV.
.36729111	.00040919	.44622619	.00202304
.44076045	.00048621	.51889021	.00210509
.51451485	.00057055	.59120894	.00198718
.58810470	.00064793	.65945588	.00153369
.66175481	.00072828	.72755451	.00170688
.73492288	.00081124	.79032413	.00116011
.80836789	.00088791	.85230234	.00128699
.88195775	.00096890	.91060621	.00135045
.95557425	.00105058	.96588232	.00164083
DETONATION FRONT		1.00000000	.00155184

YI,YF VALUES AND STANDARD DEVIATIONS FOR DATA SET NW-430

YI	STD. DEV.	YF	STD. DEV.
.31774596	.00040054	.39743485	.00262039
.39737473	.00049100	.47778639	.00145055
.47692333	.00058560	.55429109	.00157576
.55659719	.00068365	.63114778	.00169342
.63654288	.00077824	.70574471	.00171254
.71625432	.00087475	.77565178	.00149225
.79569018	.00096937	.84252496	.00150324
.87549056	.00106760	.90574045	.00133291
.95500284	.00116385	.96605359	.00135581
DETONATION FRONT		1.00000000	.00172012

YI,YF VALUES AND STANDARD DEVIATIONS FOR DATA SET NW-431

YI	STD. DEV.	YF	STD. DEV.
.25791889	.00030447	.33639766	.00289552
.34411884	.00040694	.42164128	.00268753
.42991727	.00050532	.50841910	.00275543
.51597343	.00060279	.59124001	.00313120
.60207436	.00070360	.67281295	.00216092
.68840453	.00080498	.74367228	.00170927
.77492461	.00090738	.82322133	.00189413
.86106895	.00100576	.89331695	.00162877
.94708170	.00110520	.95848170	.00176491
DETONATION FRONT		1.00000000	.00164405

YI,YF VALUES AND STANDARD DEVIATIONS FOR DATA SET NW-432

YI	STD. DEV.	YF	STD. DEV.
.19210008	.00045413	.27211438	.00218995
.28834328	.00067852	.37045285	.00224104
.38450467	.00090606	.46783990	.00258832
.48080545	.00112959	.56078187	.00163733
.57668201	.00135223	.65173614	.00200128
.67304339	.00157811	.73997397	.00209678
.76946233	.00180403	.82400914	.00231831
.86584946	.00202874	.90244479	.00239786
.96192753	.00225461	.97717773	.00253148
DETONATION FRONT		1.00000000	.00331026

YI,YF VALUES AND STANDARD DEVIATIONS FOR DATA SET NW-442

YI	STD. DEV.	YF	STD. DEV.
.10441676	.00007374	.17970039	.00367932
.20865652	.00007727	.28277496	.00307169
.31272585	.00010210	.39117239	.00281338
.41689351	.00010680	.49560717	.00295330
.52072521	.00014096	.59449950	.00163694
.62498955	.00014953	.69135807	.00166960
.72914738	.00017169	.78283150	.00141388
.83360674	.00019783	.86852486	.00196018
.93768426	.00021103	.95034735	.00142481
DETONATION FRONT		1.00000000	.00029434

YI,YF VALUES AND STANDARD DEVIATIONS FOR DATA SET NW-433

YI	STD. DEV.	YF	STD. DEV.
.11356868	.00020505	.18772673	.00355069
.22717307	.00036354	.30070805	.00365647
.34060251	.00054525	.41832581	.00336378
.45398016	.00072313	.52918440	.00282737
.56738281	.00090441	.63695620	.00183145
.68016953	.00108508	.73816163	.00308028
.79346864	.00125235	.83703368	.00224735
.90724977	.00143441	.92726841	.00262744
DETONATION FRONT		1.00000000	.00221678

YI,YF VALUES AND STANDARD DEVIATIONS FOR DATA SET NW-434

YI	STD. DEV.	YF	STD. DEV.
.57967212	.00119374	.65254794	.00218177
.69514216	.00143174	.75565228	.00234211
.81155708	.00167052	.85396818	.00237249
.92785480	.00190761	.94546307	.00231037
DETONATION FRONT		1.00000000	.00290038

YI,YF VALUES AND STANDARD DEVIATIONS FOR DATA SET NW-435

YI	STD. DEV.	YF	STD. DEV.
.13111872	.00026728	.21819611	.00362286
.26207610	.00052004	.34843367	.00322099
.39373261	.00075624	.47532035	.00206513
.52474791	.00100385	.60136517	.00305711
.65632168	.00124956	.72144874	.00161226
.78715289	.00150034	.83421208	.00234812
.91826333	.00174707	.93939457	.00289114
DETONATION FRONT		1.00000000	.00268535

APPENDIX B. INVESTIGATION OF VARIOUS FITTING FORMS

The flow variables calculated by Eqs. (3.10) to (3.15) depend upon the analytic form of y(Y). In general, different analytic forms can be expected to produce slightly different results particularly because derivatives of the fitting form are involved. Since there is no physical basis, other than very general smoothness requirements, upon which to select a fitting form, it is the purpose of this appendix to estimate the amount of variation in the flow variables that can arise due to the choice of the fitting form. The approach is straightforward; we simply try a variety of fitting forms and hope that we obtain a representative sample. Of course, we retain only those fitting forms that provide a "good" fit to the data, i.e., those forms that have essentially the same value for the standard deviation of the fit [Eq. (3.28)].

We first seek to determine the minimum number of parameters required to describe the data adequately. We consider eight two-parameter forms and eight three-parameter forms and look at the reduction in the sum of the squares of the deviations (SSD) that is achieved by introducing the additional parameter. To simplify the specification of such a wide variety of fitting forms, we utilize the fact that the specification of the form of any flow variable is equivalent to the specification of y(Y). The equations that relate the form of the specified flow variable to the form of y(Y) or Y(y) are given in Appendix C. The following fitting forms are investigated:

Two-Parameter:

$$u/D = a_1 y^{a_2} , \tag{B1a}$$

$$u/D = a_1 y + a_2 , \tag{B2a}$$

$$u/D = a_1 Y^{a_2} , \tag{B3a}$$

$$u/D = a_1 e^{a_2 Y} , \tag{B4a}$$

$$\rho/\rho_o = a_1 y^{a_2} , \tag{B5a}$$

$$\rho/\rho_o = a_1 y + a_2 , \tag{B6a}$$

$$\rho/\rho_o = a_1 Y + a_2 , \quad \rho/\rho_o = A_1 e^{A_2 y} , \tag{B7a}$$

$$\rho/\rho_o = a_1 e^{a_2 Y} , \tag{B8a}$$

Three-Parameter:

$$u/D = a_1 y^{a_2} + a_3 , \tag{B1b}$$

$$u/D = a_1 y^2 + a_2 y + a_3 , \tag{B2b}$$

$$u/D = a_1 Y^{a_2} + a_3 , \tag{B3b}$$

$$u/D = a_1 e^{a_2 Y} + a_3 , \tag{B4b}$$

$$\rho/\rho_o = a_1 y^{a_2} + a_3 , \tag{B5b}$$

$$\rho/\rho_o = a_1 y^2 + a_2 y + a_3 , \tag{B6b}$$

$$\rho/\rho_o = a_1 e^{a_2 y} + a_3 , \tag{B7b}$$

$$\rho/\rho_o = a_1 e^{a_2 Y} + a_3 . \tag{B8b}$$

The two forms given in Eq. (B7a) are equivalent analytically. The second form is given simply to show that Eq. (B7b) is a natural three-parameter extension.

In Table B-1 we list the parameter values and their standard deviations together with the reduction in the sum of the squares of the deviations that is achieved. The average reduction in SSD is 2.6%. For the three-parameter forms, the standard deviations of the parameters are generally as large as the parameters themselves. Furthermore, the off-diagonal elements of the correlation matrix are generally very close to ±1. All of this suggests that two parameters are adequate to describe the data; hence, no further consideration is given to the three-parameter forms.

The differences in the calculated flow variables for the two-parameter forms are shown in Figs. B.1. The differences are relative to the values obtained with fitting form (B7a), $\rho/\rho_o = AY + B$, which is representative of the mean. The absolute values obtained with each fitting form are listed at the detonation front in Table B-II and at the end of the Taylor wave in Table B-III. Three other forms are added:

$$y_U = a_1 Y(1-Y) + a_2(1-Y) + Y , \tag{B9}$$

$$p = a_1 (v/v_o)^{-1.34} + a_3 e^{a_4 v/v_o} + 0.076783\, e^{-1.1v/v_o} , \tag{B10}$$

$$\ell n p = a_1 + a_2 \ell n v + a_3 (\ell n v)^2 + 0.028355 (\ell n v)^3 - 0.012436 (\ell n v)^4 . \tag{B11}$$

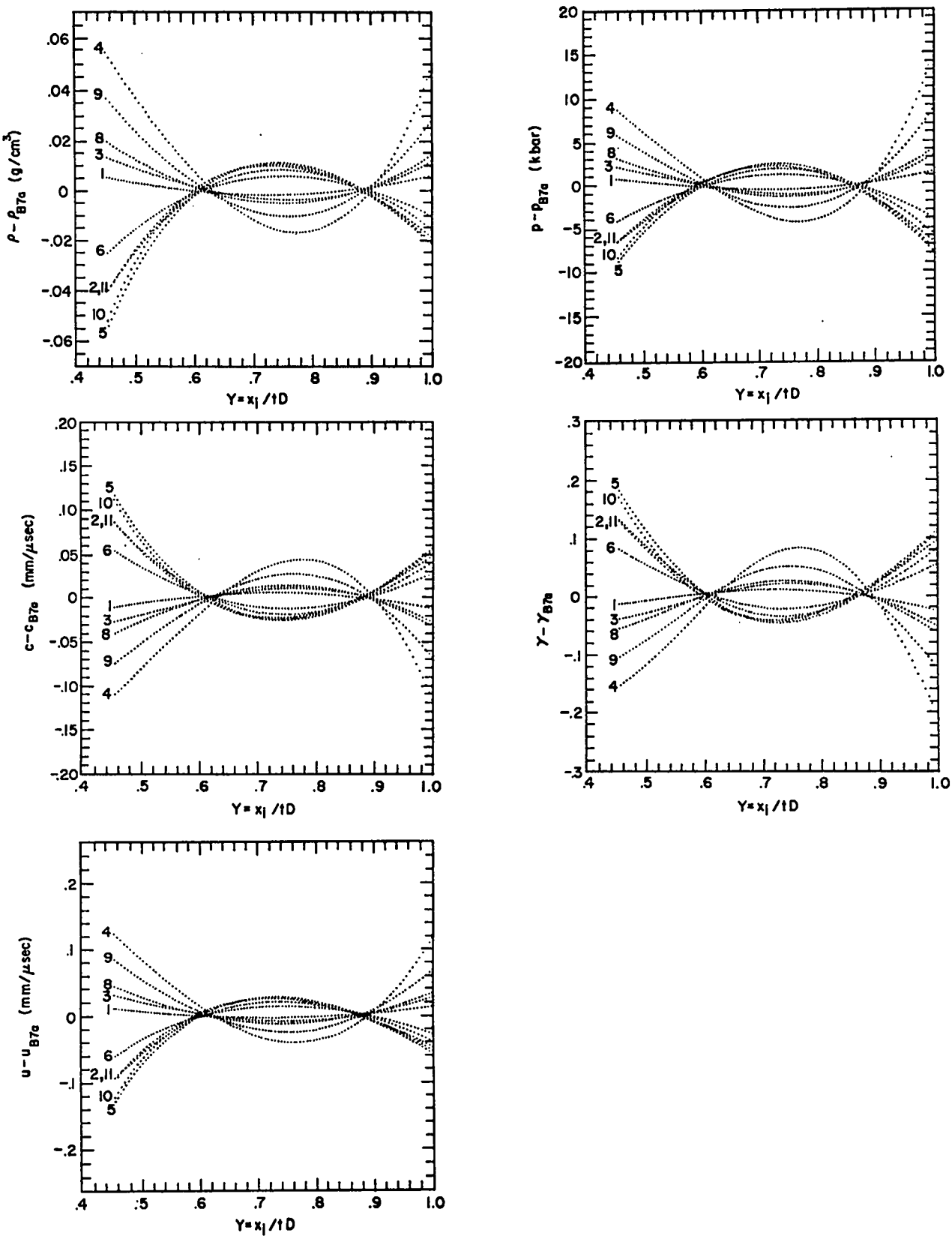

Fig. B.1. Differences in calculated flow variables for 11 fitting forms relative to fitting form (B7a).

Form (B9) is added because y_U is linear in a_1 and a_2 and, hence, their standard deviations can be calculated exactly for the analysis of variance described in Appendix E. The parameter values for this fitting form are listed at the beginning of Appendix E. Forms (B10) and (B11) are the JWL and BKW-HOM forms, respectively. The constants in each form are calibration values (see Sec. IIIB5) and a_1 is a function of the two free parameters through the Rankine-Hugoniot equations and the Chapman-Jouguet condition [see Eqs. (3.32) and (3.33)]. The values of a_1 and the two free parameters in each case are given in Table 3-III.

TABLE B-I. PARAMETERS AND STANDARD DEVIATIONS FOR TWO- AND THREE-PARAMETER FITTING FORMS TOGETHER WITH THE REDUCTION IN THE SUM OF THE SQUARES OF THE DEVIATIONS ACHIEVED BY ADDING THE THIRD PARAMETER.

The data are fitted over the range $0.454 \le Y \le 1$ (53 data points).

Fitting Form	$a_1 \pm \sigma$	$a_2 \pm \sigma$	$a_3 \pm \sigma$	% Reduction in SSD
B1	0.25695 ±0.003	1.9253 ±0.068		
	0.24986 ±0.047	2.0222 ±0.688	0.00777 ±0.052	0.04
B2	0.39888 ±0.013	-0.14877 ±0.011		
	0.26104 ±0.167	-0.91534 ±0.266	0.01205 ±0.104	4.51
B3	0.25884 ±0.003	1.5176 ±0.054		
	0.26380 ±0.056	1.4677 ±0.547	-0.00547 ±0.062	0.02
B4	0.03604 ±0.002	2.0144 ±0.072		
	0.34042 ±0.602	0.62084 ±0.547	-0.37479 ±0.653	6.40
B5	1.3304 ±0.004	0.50309 ±0.016		
	0.50590 ±0.120	1.7750 ±0.684	0.84057 ±0.128	6.99
B6	0.75277 ±0.023	0.58373 ±0.019		
	0.37186 ±0.317	0.15949 ±0.507	0.81537 ±0.199	2.62
B7	0.63388 ±0.020	0.70890 ±0.015		
	0.35748 ±0.572	0.96854 ±0.869	0.40527 ±0.698	0.30
B8	0.79023 ±0.011	0.53587 ±0.002		
	1.4406 ±3.96	0.34069 ±0.746	-0.67773 ±4.07	0.14

TABLE B-II. FLOW VARIABLES AT THE DETONATION FRONT (Y = 1) FOR THE 11 FITTING FORMS GIVEN BY EQS. (B1a to B8a), (B9), (B10), AND (B11). DATA ARE FITTED FOR $0.454 \le Y \le 1$. MEAN VALUES AND STANDARD DEVIATIONS, σ_{ff}, ARE ALSO LISTED.

Fitting Form	$\hat{\rho}/\rho_o$	$\hat{c}/D$	$\hat{u}/D$	$\hat{p}$(kbar)	$\hat{Y}$
B1a	1.3458	0.74305	0.25695	276.47	2.8918
B2a	1.3335	0.74989	0.25011	269.10	2.9983
B3a	1.3492	0.74116	0.25884	278.50	2.8634
B4a	1.3701[a]	0.72987[b]	0.27013[a]	290.65[a]	2.7019[b]
B5a	1.3304	0.75165	0.24835	267.21	3.0267
B6a	1.3365	0.74823	0.25177	270.90	2.9718
B7a(ref.)	1.3428	0.74473	0.25527	274.66	2.9174
B8a	1.3504	0.74050	0.25950	279.21	2.8535
B9	1.3586	0.73602	0.26398	284.03	2.7882
B10	1.3319	0.75082	0.24918	268.10	3.0132
B11	1.3299[b]	0.75191[a]	0.24809[b]	266.94[b]	3.0308[a]
Mean	1.3436	0.74435	0.25565	275.07	2.9143
σ_{ff}	0.0039	0.00214	0.00214	2.30	0.0322

(a) Maximum, (b) Minimum

TABLE B-III. FLOW VARIABLES AT THE END OF THE TAYLOR WAVE (Y = 0.454) FOR THE 11 FITTING FORMS GIVEN BY EQS. (B1a) to (B8a), (B9), (B10), AND (B11). DATA ARE FITTED FOR $0.454 \le Y \le 1$. MEAN VALUES AND STANDARD DEVIATIONS ARE ALSO LISTED.

Fitting Form	ρ/ρ_o	c/D	u/D	p(kbar)	Y
B1a	0.9991	0.45372	0.07546	132.15	1.6748
B2a	0.9737	0.46688	0.06231	124.99	1.8271
B3a	1.0042	0.45207	0.07808	133.61	1.6527
B4a	1.0281[a]	0.44159[b]	0.08993[a]	140.18[a]	1.5387[b]
B5a	0.9659[b]	0.47101[a]	0.05817[b]	122.77[b]	1.8780[a]
B6a	0.9821	0.46248	0.06671	127.38	1.7743
B7a(ref.)	0.9967	0.45550	0.07425	131.50	1.6919
B8a	1.0079	0.45044	0.07987	134.57	1.6350
B9	1.0179	0.44602	0.08482	137.30	1.5868
B10	0.9666	0.46969	0.05870	123.14	1.8632
B11	0.9733	0.46644	0.06226	125.02	1.8224
Mean	0.9923	0.45780	0.07187	130.24	1.7223
σ_{ff}	0.0064	0.00302	0.00328	1.79	0.0351

(a) Maximum, (b) Minimum

APPENDIX C. TECHNIQUE FOR INDIRECT SPECIFICATION OF THE LEAST-SQUARES FITTING FORM

A general least-squares algorithm capable of treating both linear and nonlinear fitting forms is used to fit the data. The algorithm involves a calculation of the partial derivatives of the fitting form, $y(Y; a_n)$ or $Y(y; a_n)$, with respect to each parameter.

The equations that define the fitting form and its partial derivatives are listed for the cases when a form is specified for $\rho(y)/\rho_o$, $\rho(Y)/\rho_o$, $u(y)/D$, $u(Y)/D$, $P(\rho_o/\rho)/\rho_o D^2$, or $\gamma(\rho/\rho_o)$. We also list the additional equations, in each case, necessary to completely describe the flow. The x, t coordinates of the negative characteristics are calculated in all case as

$$t = \tilde{x}\, Y^{-\frac{1}{2}}/D \quad , \tag{C1}$$

$$x = \tilde{x}\, y\, Y^{-\frac{1}{2}} \quad , \tag{C2}$$

where $\tilde{x}$ is the value of x at the intersection of the negative characteristic with the Chapman-Jouguet detonation front. The boundary conditions listed below correspond to an instantaneous Chapman-Jouguet detonation, i.e., the Taylor wave is attached to the detonation front. The initial conditions are

$$u_o = 0 \quad , \tag{C3}$$

$$P_o \geq 0 \quad . \tag{C4}$$

In the remainder of this appendix we use the following reduced variables $\tilde{\rho} = 1/\tilde{v} = \rho/\rho_o$, $\tilde{u} = u/D$, $\tilde{c} = c/D$, $\tilde{p} = p/\rho_o D^2$, $\tilde{E} = (E - E_o)/D^2$, and drop the tilde.

1. Specification of $\rho(y\,;\, a_n)$.

The fitting form, $Y(y)$, and the partial derivatives, $\partial Y/\partial a_\ell$, are given by

$$Y' = \rho \quad , \tag{C5}$$

$$\left(\frac{\partial Y}{\partial a_\ell}\right)' = \left(\frac{\partial \rho}{\partial a_\ell}\right)_y \quad , \tag{C6}$$

with boundary conditions

$$\hat{Y} = 1 \quad , \tag{C7}$$

$$\frac{\partial \hat{Y}}{\partial a_\ell} = 0 \quad . \tag{C8}$$

The prime denotes partial differentiation with respect to the independent variable (y, Y, ρ, or v) of the specified flow variable (ρ, u, γ, or p). The parameters are held constant during the differentiation. The ($\hat{}$) denotes a quantity evaluated at the Chapman-Jouguet point.

The additional equations are

$$p' = (Y/\rho)^2\, \rho' \quad , \tag{C9}$$

$$E' = p\, \rho^{-2}\, \rho' \quad , \tag{C10}$$

$$c = Y/\rho \quad , \tag{C11}$$

$$u = y - c \quad , \tag{C12}$$

$$\gamma = c^2\, \rho/p \quad , \tag{C13}$$

with boundary conditions

$$\hat{u} = (\hat{\rho} - 1)/\hat{\rho} \quad , \tag{C14}$$

$$\hat{p} = \hat{u} + p_o \quad , \tag{C15}$$

$$\hat{E} = p_o\, \hat{u} + \tfrac{1}{2}\, \hat{u} \quad . \tag{C16}$$

2. Specification of $\rho(Y\,;\, a_n)$.

The fitting form, $y(Y)$, and the partial derivatives, $\partial y/\partial a_\ell$, are given by

$$y' = 1/\rho \quad , \tag{C17}$$

$$\left(\frac{\partial y}{\partial a_\ell}\right)' = -\,\rho^{-2} \left(\frac{\partial \rho}{\partial a_\ell}\right)_Y \quad , \tag{C18}$$

with boundary conditions

$$\hat{y} = 1 \quad , \tag{C19}$$

$$\frac{\partial \hat{y}}{\partial a_\ell} = 0 \quad . \tag{C20}$$

The additional equations and boundary conditions are the same as in the previous case.

3. Specification of $u(y\,;\, a_n)$.

The fitting form, $Y(y)$, and the partial derivatives, $\partial Y/\partial a_\ell$, are given by

$$c = y - u \quad , \tag{C21}$$

$$\rho' = (\rho/c)\, u' \quad , \tag{C22}$$

$$Y' = \rho \quad , \tag{C23}$$

$$\frac{\partial c}{\partial a_\ell} = \left(\frac{\partial u}{\partial a_\ell}\right)_y \quad , \tag{C24}$$

$$\left(\frac{\partial \rho}{\partial a_\ell}\right)' = \frac{1}{c}\left[\rho \left(\frac{\partial u'}{\partial a_\ell}\right)_y + u' \frac{\partial \rho}{\partial a_\ell} - \frac{\rho u'}{c} \frac{\partial c}{\partial a_\ell}\right] \quad , \tag{C25}$$

$$\left(\frac{\partial \gamma}{\partial a_\ell}\right)' = \frac{\partial \rho}{\partial a_\ell} \quad , \tag{C26}$$

with boundary conditions

$$\hat{\rho} = 1/(1 - \hat{u}) \quad , \tag{C27}$$

$$\hat{Y} = 1 \quad , \tag{C28}$$

$$\frac{\partial \hat{\rho}}{\partial a_\ell} = (1 - \hat{u})^{-2} \left(\frac{\partial \hat{u}}{\partial a_\ell}\right)_y \quad , \tag{C29}$$

$$\frac{\partial \hat{Y}}{\partial a_\ell} = 0 \quad . \tag{C30}$$

The additional equations are

$$p' = c^2 \rho' \quad , \tag{C31}$$

$$E' = p\, \rho^{-2} \rho' \quad , \tag{C32}$$

$$\gamma = c^2 \rho / p \quad , \tag{C33}$$

with boundary conditions

$$\hat{p} = \hat{u} + p_o \quad , \tag{C34}$$

$$\hat{E} = p_o \hat{u} + \tfrac{1}{2} \hat{u}^2 \quad . \tag{C35}$$

4. Specification of $u(Y\ ;\ a_n)$.

The fitting form, $y(Y)$, and the partial derivatives, $\partial y/\partial a_\ell$, are given by

$$c = Y/\rho \quad , \tag{C36}$$

$$\rho' = \rho\, u'/c \quad , \tag{C37}$$

$$y' = 1/\rho \quad , \tag{C38}$$

$$\left(\frac{\partial c}{\partial a_\ell}\right) = - Y \rho^{-2} \left(\frac{\partial \rho}{\partial a_\ell}\right) \quad , \tag{C39}$$

$$\left(\frac{\partial \rho}{\partial a_\ell}\right)' = \frac{1}{c}\left[\rho \left(\frac{\partial u'}{\partial a_\ell}\right)_Y + u' \frac{\partial \rho}{\partial a_\ell} - \frac{\rho u'}{c} \frac{\partial c}{\partial a_\ell}\right] \quad , \tag{C40}$$

$$\left(\frac{\partial y}{\partial a_\ell}\right)' = - \rho^{-2} \left(\frac{\partial \rho}{\partial a_\ell}\right) \quad , \tag{C41}$$

with boundary conditions

$$\hat{\rho} = 1/(1 - \hat{u}) \quad , \tag{C42}$$

$$\hat{y} = 1 \quad , \tag{C43}$$

$$\frac{\partial \hat{\rho}}{\partial a_\ell} = (1 - \hat{u})^{-2} \left(\frac{\partial \hat{u}}{\partial a_\ell}\right)_Y \quad , \tag{C44}$$

$$\frac{\partial \hat{y}}{\partial a_\ell} = 0 \quad . \tag{C45}$$

The additional equations and boundary conditions are the same as for $u(y)$.

5. Specification of $\gamma(\rho\ ;\ a_n)$.

The fitting form, $y(Y)$, and the partial derivatives, $\partial y/\partial a_\ell$, are given by

$$c = Y/\rho \quad , \tag{C46}$$

$$F(\rho) \equiv \gamma(1 + \gamma) + \rho\, \gamma' \quad , \tag{C47}$$

$$\frac{d\rho}{dY} = \frac{2\gamma}{cF} \quad , \tag{C48}$$

$$\frac{dy}{dY} = \frac{1}{\rho} \quad , \tag{C49}$$

$$\left(\frac{\partial \gamma}{\partial a_\ell}\right)_Y = \left(\frac{\partial \gamma}{\partial a_\ell}\right)_\rho + \gamma' \left(\frac{\partial \rho}{\partial a_\ell}\right)_Y \quad , \tag{C50}$$

$$\left(\frac{\partial \gamma'}{\partial a_\ell}\right)_Y = \left(\frac{\partial \gamma'}{\partial a_\ell}\right)_\rho + \gamma'' \left(\frac{\partial \rho}{\partial a_\ell}\right)_Y \quad , \tag{C51}$$

$$\left(\frac{\partial F}{\partial a_\ell}\right)_Y = \left(\frac{\partial \gamma}{\partial a_\ell}\right)_Y (1 + 2\gamma) + \rho \left(\frac{\partial \gamma'}{\partial a_\ell}\right)_Y + \gamma' \left(\frac{\partial \rho}{\partial a_\ell}\right)_Y \tag{C52}$$

$$\left(\frac{\partial c}{\partial a_\ell}\right)_Y = Y \rho^{-2} \left(\frac{\partial \rho}{\partial a_\ell}\right)_Y \quad , \tag{C53}$$

$$\frac{d}{dY}\left(\frac{\partial \rho}{\partial a_\ell}\right)_Y = \frac{2}{cF}\left(\frac{\partial \gamma}{\partial a_\ell}\right)_Y - \frac{2\gamma F^{-2}}{c}\left(\frac{\partial F}{\partial a_\ell}\right)_Y - \frac{2\gamma c^{-2}}{F}\left(\frac{\partial c}{\partial a_\ell}\right)_Y \quad , \tag{C54}$$

$$\frac{d}{dY}\left(\frac{\partial y}{\partial a_\ell}\right)_Y = - \rho^{-2} \left(\frac{\partial \rho}{\partial a_\ell}\right)_Y \quad . \tag{C55}$$

The value of $\hat{\rho}$ is given by

$$\gamma\,(\hat{\rho}\ ;\ a_n) - (\hat{\rho} - 1 + p_o\, \hat{\rho})^{-1} = 0 \quad . \tag{C56}$$

The other boundary conditions are

$$\hat{y} = 1 \quad , \tag{C57}$$

$$\left(\frac{\partial \hat{\rho}}{\partial a_\ell}\right)_Y = - \left(\frac{\partial \hat{Y}}{\partial a_\ell}\right)_\rho \left[\hat{Y}' + \hat{Y}^2\, (1 + p_o)\right]^{-1} \quad , \tag{C58}$$

$$\left(\frac{\partial \hat{y}}{\partial a_\ell}\right)_Y = 0 \quad . \tag{C59}$$

The additional equations are

$$\frac{du}{dY} = \frac{c}{\rho} \frac{d\rho}{dY} \quad , \tag{C60}$$

$$\frac{dp}{dY} = c^2 \frac{d\rho}{dY} \quad , \tag{C61}$$

$$\frac{dE}{dY} = p\, \rho^{-2} \frac{d\rho}{dY} \quad , \tag{C62}$$

with boundary conditions

$$\hat{u} = (\hat{\rho} - 1)/\hat{\rho} \quad , \tag{C63}$$

$$\hat{p} = u + \hat{p}_o \quad , \tag{C64}$$

$$\hat{E} = p_o \hat{u} + \tfrac{1}{2} \hat{u}^2 \quad . \tag{C65}$$

6. Specification of $p(v;a_n)$

The fitting form, $y(Y)$, and the partial derivatives, $\partial y/\partial a_\ell$, are given by

$$c = Yv \quad , \tag{C66}$$

$$\gamma = - \frac{v}{p} p' \quad , \tag{C67}$$

$$\gamma' = - \frac{v}{p} p'' - \frac{p'}{p} + v \left(\frac{p'}{p}\right)^2 \quad , \tag{C68}$$

$$\frac{d\gamma}{d\rho} = - v^2 \gamma' \quad , \tag{C69}$$

$$F(\rho) \equiv \gamma (1 + \gamma) + \rho \frac{d\gamma}{d\rho} \quad , \tag{C70}$$

$$\frac{d\rho}{dY} = \frac{2\gamma}{cF} \quad , \tag{C71}$$

$$\frac{dy}{dY} = \frac{1}{\rho} \quad , \tag{C72}$$

$$\left(\frac{\partial p}{\partial a_\ell}\right)_{v,a_k} = \left(\frac{\partial p}{\partial a_\ell}\right)_v - \left(\frac{\partial p}{\partial a_m}\right)_v \left(\frac{\partial \hat{p}}{\partial a_\ell}\right)_v \left(\frac{\partial \hat{p}}{\partial a_m}\right)_v^{-1} \quad . \tag{C73}$$

The following definitions are used in the above and all following equations.

a_m = the dependent parameter. This parameter depends upon all the other parameters.

a_ℓ = any parameter except a_m.

a_k = all parameters except a_m and a_ℓ.

Partial differentiation with respect to a parameter implies that all the other parameters are held fixed unless otherwise noted.

$$\left(\frac{\partial p'}{\partial a_\ell}\right)_{v,a_k} = \left(\frac{\partial p'}{\partial a_\ell}\right)_v - \left(\frac{\partial p'}{\partial a_m}\right)_v \left(\frac{\partial \hat{p}}{\partial a_\ell}\right)_v \left(\frac{\partial \hat{p}}{\partial a_m}\right)_v^{-1} \quad , \tag{C74}$$

$$\left(\frac{\partial p''}{\partial a_\ell}\right)_{v,a_k} = \left(\frac{\partial p''}{\partial a_\ell}\right)_v - \left(\frac{\partial p''}{\partial a_m}\right)_v \left(\frac{\partial \hat{p}}{\partial a_\ell}\right)_v \left(\frac{\partial \hat{p}}{\partial a_m}\right)_v^{-1} \quad , \tag{C75}$$

$$\left(\frac{\partial \gamma}{\partial a_\ell}\right)_{v,a_k} = \left[\left(\frac{\partial p}{\partial a_\ell}\right)_{v,a_k} v\, p' - pv \left(\frac{\partial p'}{\partial a_\ell}\right)_{v,a_k}\right] p^{-2} \quad , \tag{C76}$$

$$\left(\frac{\partial \gamma}{\partial a_\ell}\right)_{Y,a_k} = \left(\frac{d\gamma}{d\rho}\right)\left(\frac{\partial \rho}{\partial a_\ell}\right)_{Y,a_k} + \left(\frac{\partial \gamma}{\partial a_\ell}\right)_{v,a_k} \quad , \tag{C77}$$

$$\gamma'' = - \frac{v}{p} p''' - \frac{2}{p} p'' + \frac{3v}{p^2} p' p'' + \frac{2(p - vp')}{p^3} (p')^2 \quad , \tag{C78}$$

$$\frac{d^2\gamma}{d\rho^2} = v^4 \gamma'' + 2 v^3 \gamma' \quad , \tag{C79}$$

$$\left(\frac{\partial \gamma'}{\partial a_\ell}\right)_{v,a_k} = \frac{-v}{p}\left(\frac{\partial p''}{\partial a_\ell}\right)_{v,a_k} + \frac{vp''}{p^2}\left(\frac{\partial p}{\partial a_\ell}\right)_{v,a_k} - \frac{1}{p}\left(\frac{\partial p'}{\partial a_\ell}\right)_{v,a_k} + \frac{p'}{p^2}\left(\frac{\partial p}{\partial a_\ell}\right)_{v,a_k} + \frac{2vp'}{p^2}\left(\frac{\partial p'}{\partial a_\ell}\right)_{v,a_k} - \frac{2v(p')^2}{p^3}\left(\frac{\partial p}{\partial a_\ell}\right)_{v,a_k} \tag{C80}$$

$$\left(\frac{\partial}{\partial a_\ell}\left(\frac{d\gamma}{d\rho}\right)\right)_{v,a_k} = - v^2 \left(\frac{\partial \gamma'}{\partial a_\ell}\right)_{v,a_k} \quad , \tag{C81}$$

$$\left(\frac{\partial}{\partial a_\ell}\left(\frac{d\gamma}{d\rho}\right)\right)_{Y,a_k} = \frac{d^2\gamma}{d\rho^2}\left(\frac{\partial \rho}{\partial a_\ell}\right)_{Y,a_k} + \left(\frac{\partial}{\partial a_\ell}\left(\frac{d\gamma}{d\rho}\right)\right)_{v,a_k} \quad , \tag{C82}$$

$$\left(\frac{\partial F}{\partial a_\ell}\right)_{Y,a_k} = \left(\frac{\partial \gamma}{\partial a_\ell}\right)_{Y,a_k} (1 + 2\gamma) + \rho \left(\frac{\partial}{\partial a_\ell}\left(\frac{d\gamma}{d\rho}\right)\right)_{Y,a_k} + \frac{d\gamma}{d\rho}\left(\frac{\partial \rho}{\partial a_\ell}\right)_{Y,a_k} \quad , \tag{C83}$$

$$\left(\frac{\partial c}{\partial a_\ell}\right)_{Y,a_k} = - Y \rho^{-2} \left(\frac{\partial \rho}{\partial a_\ell}\right)_{Y,a_k} \quad , \tag{C84}$$

$$\frac{d}{dY}\left(\frac{\partial \rho}{\partial a_\ell}\right)_{Y,a_k} = \frac{2}{cF}\left(\frac{\partial \gamma}{\partial a_\ell}\right)_{Y,a_k} - \frac{2\gamma}{cF^2}\left(\frac{\partial F}{\partial a_\ell}\right)_{Y,a_k} - \frac{2\gamma}{c^2 F}\left(\frac{\partial c}{\partial a_\ell}\right)_{Y,a_k} \quad , \tag{C85}$$

$$\frac{d}{dY}\left(\frac{\partial y}{\partial a_\ell}\right)_{Y,a_k} = - \rho^{-2} \left(\frac{\partial \rho}{\partial a_\ell}\right)_{Y,a_k} \quad . \tag{C86}$$

The values of v and a_m are obtained by simultaneous solution of

$$p'(\hat{v} \; ; \; a_k, \; a_m) = -1 \quad , \tag{C87}$$

$$p(\hat{v} \; ; \; a_k, \; a_m) = 1 - \hat{v} + p_o \quad . \tag{C88}$$

The other boundary conditions are

$$\hat{p} = 1/\hat{v} \quad ,$$

$$\hat{\gamma} = - \frac{\hat{v}}{\hat{p}} \hat{p}' \quad , \tag{C90}$$

$$\hat{y} = 1 \quad , \tag{C91}$$

$$\left(\frac{\partial \hat{p}}{\partial a_\ell}\right)_{Y, a_k} = \left(\frac{\partial \hat{v}}{\partial a_\ell}\right)_{v, a_k} \left[\frac{d\hat{\gamma}}{d\rho} + \hat{\gamma}^2 (1 + p_o)\right]^{-1} \quad , \tag{C92}$$

$$\left(\frac{\partial \hat{y}}{\partial a_\ell}\right)_{Y, a_k} = 0 \quad . \tag{C93}$$

The additional equations and boundary conditions are the same as for $\gamma(\rho)$.

APPENDIX D. CALCULATED FLOW FOR THE CHAPMAN-JOUGUET/TAYLOR WAVE MODEL

The results of the Chapman-Jouguet/Taylor wave calculation are presented in this appendix for the fitting form given by Eq. (3.21), i.e.,

$$y = 1 + A^{-1} \ln \left(\frac{AY + B}{A + B}\right) \quad .$$

The results are displayed in 17 curves (Fig. D.1) followed by the tabulated values. The detonation velocity used here is 7.8863 mm/μsec and the density of the unreacted explosive is 1.730 g/cm^3. The data points that deviate from the least-squares curve, Eq. (3.21), by more than the standard deviations given in Appendix A are listed in Table D-I.

TABLE D-I. DATA POINTS THAT DEVIATE FROM THE LEAST-SQUARES FIT, EQ. (3.21), BY MORE THAN THE STANDARD DEVIATIONS GIVEN IN APPENDIX A. DATA POINTS THAT LIE BELOW THE CALCULATED CURVE HAVE A MINUS SIGN.

Data Point No.	Data Set	X	Dev/σ
31	NW-427	100.8121	-1.02
38	"	"	-1.67
52	"	"	-1.09
26	NW-428	92.5010	1.14
40	"	"	-1.73
20	NW-439	86.3013	1.47
27	"	"	1.05
35	"	"	1.17
29	NW-430	79.8317	1.69
37	"	"	1.57
53	"	"	1.06
32	NW-431	73.7193	-3.11
7	NW-442	61.0199	-1.80
16	"	"	-1.23
34	NW-433	56.0128	-1.18
45	"	"	-1.45

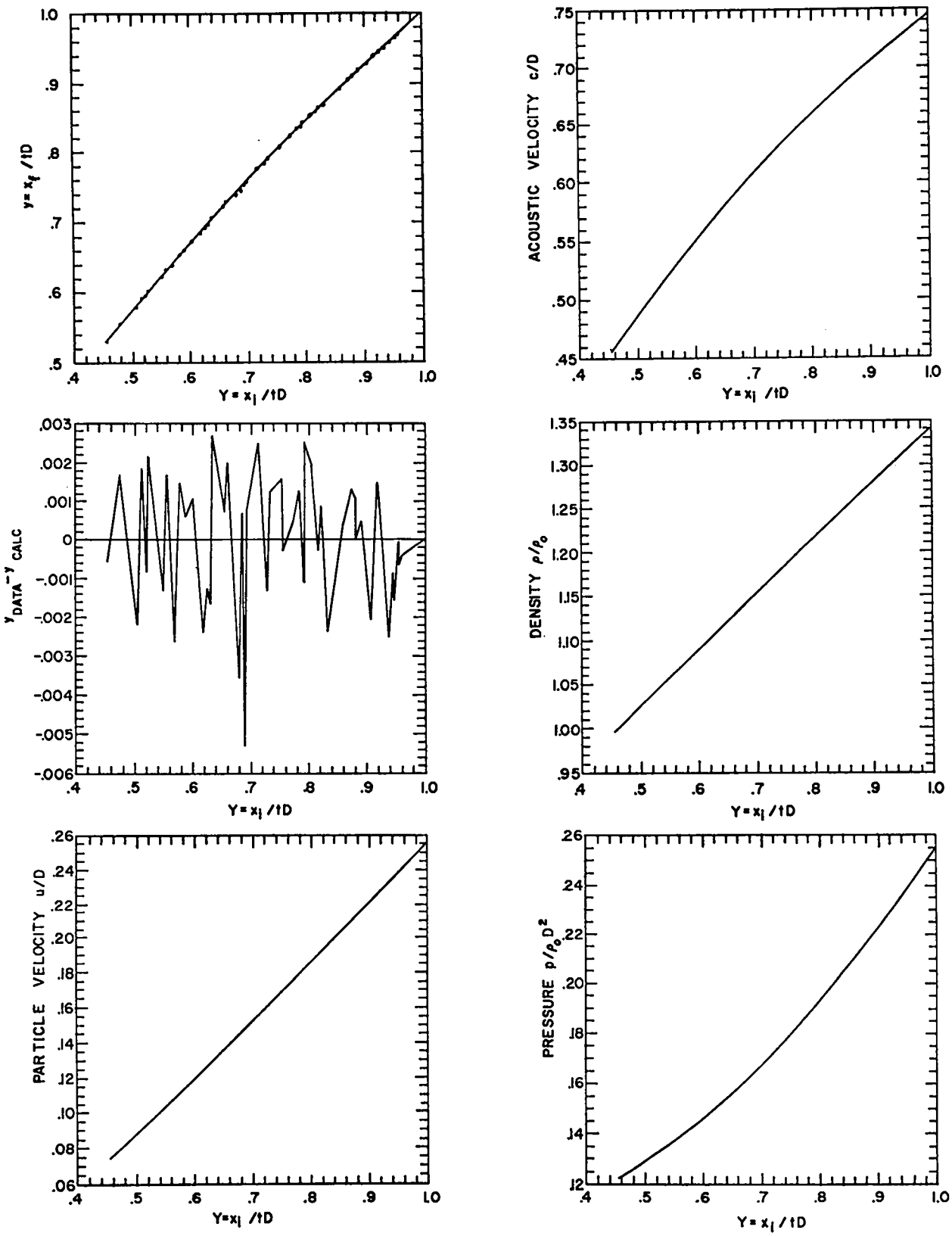

Fig. D.1. Flow variables calculated with the classical model and fitting form Eq. (3.21).

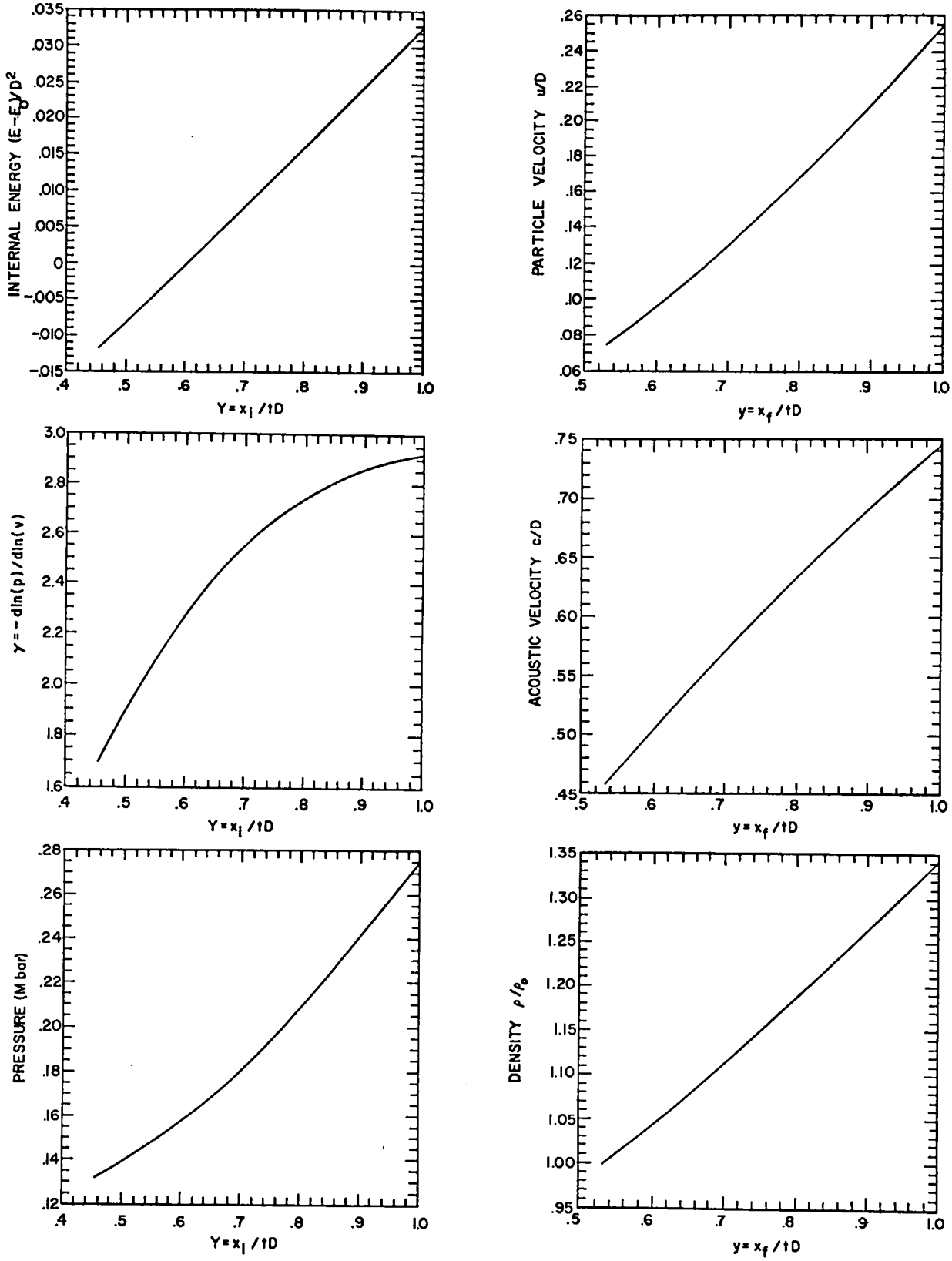

Fig. D.1 continued

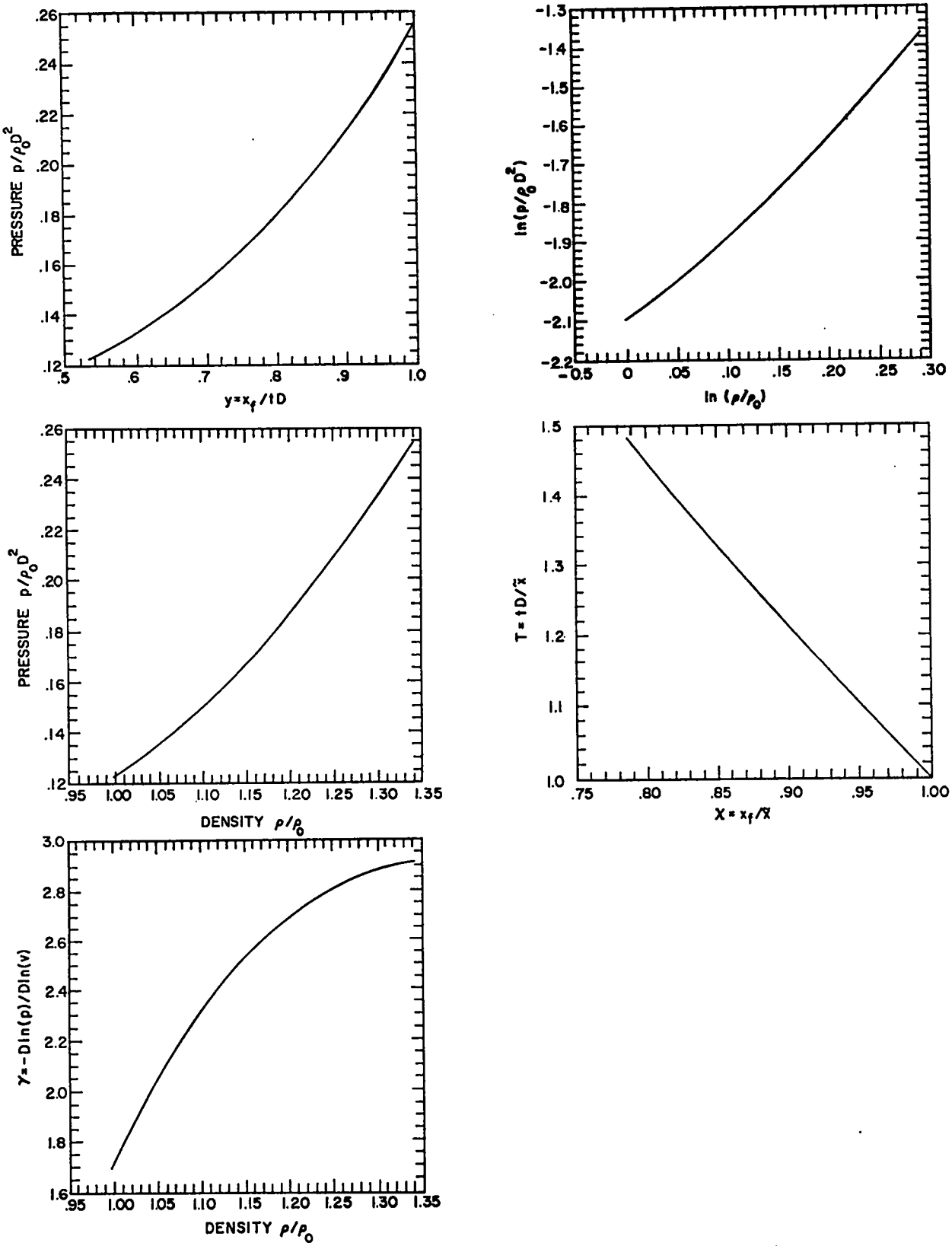

Fig. D.1 continued

FLOW FIELD FOR A SELF-SIMILAR FLOW ALL DATA SETS EXCEPT NW-432

X(I)/TD	U/D	C/D	RHO/RHO0	X/TD	P/(DD)RHO0	P(MEGABARS)	GAMMA	(E-E0)/DD
1.00000	.25527	.74473	1.34277	1.00000	.25527	.27466	2.91738	.03258
.96123	.24166	.72920	1.31820	.97086	.24192	.26030	2.89732	.02913
.95557	.23968	.72689	1.31461	.96656	.24002	.25825	2.89386	.02863
.95500	.23948	.72665	1.31425	.96613	.23983	.25805	2.89350	.02858
.94708	.23670	.72339	1.30923	.96009	.23719	.25521	2.88840	.02789
.94509	.23601	.72257	1.30797	.95857	.23653	.25450	2.88708	.02771
.93768	.23341	.71948	1.30327	.95290	.23409	.25187	2.88198	.02706
.92785	.22997	.71536	1.29704	.94534	.23089	.24842	2.87481	.02621
.91826	.22662	.71130	1.29096	.93792	.22779	.24509	2.86737	.02537
.90725	.22278	.70659	1.28398	.92937	.22428	.24132	2.85824	.02442
.89262	.21768	.70025	1.27471	.91793	.21969	.23638	2.84514	.02317
.88223	.21406	.69570	1.26812	.90976	.21649	.23293	2.83513	.02228
.88196	.21397	.69558	1.26795	.90955	.21640	.23284	2.83486	.02225
.87549	.21172	.69272	1.26385	.90444	.21443	.23071	2.82832	.02170
.86107	.20672	.68627	1.25471	.89299	.21008	.22604	2.81285	.02048
.83361	.19721	.67373	1.23730	.87094	.20203	.21738	2.77991	.01817
.82387	.19386	.66920	1.23113	.86306	.19925	.21438	2.76707	.01736
.81945	.19233	.66713	1.22833	.85946	.19800	.21304	2.76104	.01699
.81156	.18962	.66340	1.22332	.85302	.19578	.21065	2.74993	.01633
.80837	.18852	.66189	1.22130	.85041	.19490	.20970	2.74533	.01607
.79569	.18417	.65582	1.21327	.84000	.19141	.20594	2.72631	.01502
.79347	.18341	.65475	1.21186	.83817	.19080	.20529	2.72286	.01484
.78715	.18125	.65169	1.20786	.83295	.18909	.20346	2.71285	.01432
.77492	.17708	.64571	1.20010	.82279	.18583	.19995	2.69265	.01332
.75649	.17080	.63655	1.18842	.80735	.18103	.19478	2.66005	.01181
.75525	.17038	.63593	1.18763	.80631	.18071	.19444	2.65777	.01171

.73492	.16350	.62560	1.$\bar{1}$7475	.78910	.17558	.18892	2.61852	.01007
.72915	.16155	.62262	1.17109	.78418	.17416	.18$\bar{7}$38	2.60676	.00960
.71625	.15722	.61591	1.16291	.77313	.17102	.18401	2.5794$\bar{8}$	.00857
.69514	.15015	.60472	1.14953	.75487	.16604	.17865	2.53174	.00688
.69359	.14963	.60389	1.$\bar{1}$4855	.75352	.16568	.17$\bar{8}$26	2.52809	.00676
.68840	.14791	.60109	1.14526	.74900	.16449	.17$\bar{6}$98	2.51568	.00634
.68647	.14726	.60004	1.14404	.74731	.16404	.17650	2.5110$\bar{0}$	.00619
.68017	.14517	.59662	1.$\bar{1}$4004	.74179	.16261	.17496	2.4955$\bar{0}$	.00569
.66175	.13908	.58647	1.$\bar{1}$2837	.72555	.15853	.17$\bar{0}$57	2.44814	.00423
.65632	.13730	.58344	1.12492	.72073	.15735	.16$\bar{9}$30	2.43357	.00380
.63654	.13082	.57223	1.$\bar{1}$1239	.70305	.15316	.16480	2.3781$\bar{8}$	.00225
.63058	.12868	.56881	1.10861	.69768	.15193	.16347	2.36076	.00178
.62499	.12706	.56557	1.10506	.69263	.15079	.16225	2.3441$\bar{0}$	.00134
.61785	.12475	.56141	1.$\bar{1}$0054	.68616	.14936	.16$\bar{0}$70	2.32242	.00079
.60207	.11967	.55209	1.$\bar{0}$9054	.67176	.14626	.15$\bar{7}$36	2.27272	-.00045
.58810	.11520	.54369	1.$\bar{0}$8168	.65889	.14360	.15450	2.2267$\bar{0}$	-.00153
.57967	.11252	.53856	1.$\bar{0}$7634	.65108	.14203	.15282	2.1980$\bar{0}$	-.00219
.56765	.10872	.53115	1.06872	.63987	.13985	.15$\bar{0}$47	2.1559$\bar{0}$	-.00312
.56738	.10863	.53098	1.06855	.63962	.13980	.15$\bar{0}$42	2.15494	-.00314
.55660	.10525	.52425	1.$\bar{0}$6171	.62949	.13790	.14838	2.11595	-.00398
.54922	.10295	.51959	1.05704	.62253	.13663	.14$\bar{7}$01	2.08866	-.00455
.52475	.09538	.50383	1.04152	.59921	.13256	.14$\bar{2}$63	1.99436	-.00645
.52073	.09415	.50119	1.03897	.59534	.13192	.14$\bar{1}$94	$\bar{1}$.97833	-.00676
.51597	.09270	.49806	1.03596	.59076	.13117	.14$\bar{1}$13	$\bar{1}$.95920	-.00713
.51451	.09225	.49710	1.03504	.58935	.13094	.14$\bar{0}$89	$\bar{1}$.95329	-.00724
.50464	.08926	.49053	1.$\bar{0}$2878	.57979	.12941	.13924	$\bar{1}$.91278	-.00801
.47692	.08097	.47164	1.01121	.55261	.12535	.13487	1.7945$\bar{1}$	-.01016
.45398	.07425	.45550	.99667	.52975	.12222	.13$\bar{1}$50	1.69193	-.01194

FINAL RESULTS CONTINUED ALL DATA SETS EXCEPT NW-432

CROSS CHARACTERISTIC

X/XTILDE	TD/XTILDE	X/XTILDE	TD/XTILDE	X/XTILDE	TD/XTILDE
1.00000	1.00000	.94169	1.12106	.86574	1.28877
.99024	1.01997	.94095	1.12263	.85919	1.30399
.98878	1.02298	.93883	1.12712	.85515	1.31344
.98863	1.02329	.93467	1.13598	.84928	1.32727
.98655	1.02756	.92824	1.14974	.84915	1.32754
.98602	1.02864	.92781	1.15068	.84376	1.34038
.98405	1.03269	.92047	1.16648	.84062	1.34935
.98140	1.03815	.91835	1.17110	.82718	1.38046
.97878	1.04356	.91352	1.18159	.82501	1.38576
.97572	1.04987	.90539	1.19940	.82243	1.39215
.97158	1.05844	.90478	1.20074	.82163	1.39412
.96858	1.06466	.90273	1.20525	.81616	1.40769
.96850	1.06482	.90196	1.20695	.80019	1.44802
.96661	1.06875	.89944	1.21253	.78624	1.48416
.96233	1.07766	.89191	1.22928		
.95392	1.09527	.88964	1.23436		
.95085	1.10172	.88120	1.25339		
.94943	1.10469	.87859	1.25930		
.94689	1.11004	.87612	1.26492		
.94580	1.11223	.87294	1.27221		

I	WEIGHT	INDEPENDENT VARIABLE	DEPENDENT VARIABLE	CALCULATED FUNCTION	DEVIATION
1	1.0000000E+00	1.0000000E+00	1.0000000E+00	1.0000000E+00	0.
2	1.0000000E+00	9.6122850E-01	9.7043820E-01	9.7085831E-01	-4.2010810E-04
3	1.0000000E+00	9.5557420E-01	9.6588230E-01	9.6656305E-01	-6.8074817E-04
4	1.0000000E+00	9.5500280E-01	9.6605360E-01	9.6612834E-01	-7.4735770E-05
5	1.0000000E+00	9.4708170E-01	9.5848170E-01	9.6008971E-01	-1.6080111E-03
6	1.0000000E+00	9.4509390E-01	9.5768460E-01	9.5857068E-01	-8.8608317E-04
7	1.0000000E+00	9.3768430E-01	9.5034730E-01	9.5289553E-01	-2.5482266E-03
8	1.0000000E+00	9.2785480E-01	9.4546310E-01	9.4533528E-01	1.2782244E-04
9	1.0000000E+00	9.1826330E-01	9.3939460E-01	9.3792299E-01	1.4716074E-03
10	1.0000000E+00	9.0724980E-01	9.2726840E-01	9.2936861E-01	-2.1002130E-03
11	1.0000000E+00	8.9261950E-01	9.1841710E-01	9.1793279E-01	4.8431237E-04
12	1.0000000E+00	8.8223040E-01	9.0975190E-01	9.0976148E-01	-9.5814673E-06
13	1.0000000E+00	8.8195770E-01	9.1060620E-01	9.0954642E-01	1.0597755E-03
14	1.0000000E+00	8.7549060E-01	9.0574050E-01	9.0443772E-01	1.3027772E-03
15	1.0000000E+00	8.6106890E-01	8.9331690E-01	8.9298533E-01	3.3156922E-04
16	1.0000000E+00	8.3360670E-01	8.6852490E-01	8.7094477E-01	-2.4198717E-03
17	1.0000000E+00	8.2387330E-01	8.6392040E-01	8.6305846E-01	8.6194469E-04
18	1.0000000E+00	8.1945020E-01	8.5914390E-01	8.5946165E-01	-3.1774672E-04
19	1.0000000E+00	8.1155710E-01	8.5396820E-01	8.5302263E-01	9.4556683E-04
20	1.0000000E+00	8.0836790E-01	8.5230230E-01	8.5041348E-01	1.8888176E-03
21	1.0000000E+00	7.9569020E-01	8.4252500E-01	8.3999871E-01	2.5262907E-03
22	1.0000000E+00	7.9346860E-01	8.3703370E-01	8.3816656E-01	-1.1328565E-03
23	1.0000000E+00	7.8715290E-01	8.3421210E-01	8.3294635E-01	1.2657522E-03
24	1.0000000E+00	7.7492460E-01	8.2322130E-01	8.2278975E-01	4.3155412E-04
25	1.0000000E+00	7.5648560E-01	8.0703800E-01	8.0734994E-01	-3.1193673E-04
26	1.0000000E+00	7.5525130E-01	8.0788320E-01	8.0631099E-01	1.5722147E-03
27	1.0000000E+00	7.3492290E-01	7.9032410E-01	7.8910072E-01	1.2233753E-03
28	1.0000000E+00	7.2914740E-01	7.8283150E-01	7.8417667E-01	-1.3451745E-03
29	1.0000000E+00	7.1625430E-01	7.7565180E-01	7.7312856E-01	2.5232359E-03
30	1.0000000E+00	6.9514220E-01	7.5565230E-01	7.5486882E-01	7.8347665E-04
31	1.0000000E+00	6.9359330E-01	7.5254060E-01	7.5352083E-01	-9.8022967E-04
32	1.0000000E+00	6.8840450E-01	7.4367230E-01	7.4899665E-01	-5.3243531E-03
33	1.0000000E+00	6.8647040E-01	7.4797570E-01	7.4730696E-01	6.6873660E-04
34	1.0000000E+00	6.8016950E-01	7.3816160E-01	7.4178972E-01	-3.6281165E-03

35	1.0000000E+00	6.6175480E-01	7.2755450E-01	7.2555379E-01	2.0007067E-03
36	1.0000000E+00	6.5632170E-01	7.2144870E-01	7.2073143E-01	7.1727458E-04
37	1.0000000E+00	6.3654290E-01	7.0574470E-01	7.0305038E-01	2.6943200E-03
38	1.0000000E+00	6.3058400E-01	6.9598890E-01	6.9768441E-01	-1.6955074E-03
39	1.0000000E+00	6.2498960E-01	6.9135810E-01	6.9263000E-01	-1.2719005E-03
40	1.0000000E+00	6.1785390E-01	6.8371690E-01	6.8615948E-01	-2.4425759E-03
41	1.0000000E+00	6.0207440E-01	6.7281300E-01	6.7175597E-01	1.0570271E-03
42	1.0000000E+00	5.8810470E-01	6.5945590E-01	6.5889377E-01	5.6212672E-04
43	1.0000000E+00	5.7967210E-01	6.5254790E-01	6.5107864E-01	1.4692627E-03
44	1.0000000E+00	5.6765210E-01	6.3869520E-01	6.3987143E-01	-1.1762313E-03
45	1.0000000E+00	5.6738280E-01	6.3695620E-01	6.3961943E-01	-2.6632273E-03
46	1.0000000E+00	5.5659720E-01	6.3114780E-01	6.2949331E-01	1.6544946E-03
47	1.0000000E+00	5.4922430E-01	6.2118790E-01	6.2253362E-01	-1.3457243E-03
48	1.0000000E+00	5.2474790E-01	6.0136520E-01	5.9920636E-01	2.1588371E-03
49	1.0000000E+00	5.2072520E-01	5.9449950E-01	5.9533930E-01	-8.3980345E-04
50	1.0000000E+00	5.1597340E-01	5.9124000E-01	5.9075911E-01	4.8089220E-04
51	1.0000000E+00	5.1451490E-01	5.9120890E-01	5.8935061E-01	1.8582919E-03
52	1.0000000E+00	5.0464480E-01	5.7756760E-01	5.7978568E-01	-2.2180812E-03
53	1.0000000E+00	4.7692330E-01	5.5429110E-01	5.5260692E-01	1.6841815E-03
54	1.0000000E+00	4.5398020E-01	5.2918440E-01	5.2975339E-01	-5.6898887E-04

APPENDIX E. ANALYSIS OF VARIANCE

In this appendix we calculate the variances in ρ, c, u, p, and γ that arise from the variances in the fit parameters and the variance in the detonation velocity. To this end we use fitting form (B9)

$$y = AY(1 - Y) + B(1 - Y) + Y \quad , \tag{E1}$$

where A = 0.22567 and B = 0.038308. The statistical analysis of the least-squares fit applies exactly for this form since it is linear in A and B. The correlation coefficient and standard deviations of the parameters are

$$r_{AB} = -0.98528 \quad , \tag{E2}$$

$$\sigma(A) = 7.3275 \times 10^{-3} \quad , \tag{E3}$$

$$\sigma(B) = 4.4746 \times 10^{-3} \quad . \tag{E4}$$

The standard deviation of the mean detonation velocity is

$$\sigma(D) = 7.7338 \times 10^{-3} \text{ mm}/\mu\text{sec} \quad . \tag{E5}$$

The variances V(A), V(B), V(D), and the covariance V(A,B) are given by

$$V(A) = \sigma(A)^2 \quad , \tag{E6}$$

$$V(B) = \sigma(B)^2 \quad , \tag{E7}$$

$$V(D) = \sigma(D)^2 \quad , \tag{E8}$$

$$V(A,B) = r_{AB}\, \sigma(A)\sigma(B) \quad . \tag{E9}$$

The variances in the flow variables are calculated as follows.

1. Variance in Density.

The density, given by Eqs. (E1) and (3.10), is $\rho = \rho_o[A(1 - 2Y) + 1 - B]^{-1}$, and its variance is

$$V(\rho\ ;\ Y) = \rho_A^2\, V(A) + \rho_B^2\, V(B) + 2\rho_A\rho_B\, V(A,B) \quad , \tag{E10}$$

where

$$\rho_A = (2Y - 1)\rho^2/\rho_o \quad , \quad \rho_B = \rho^2/\rho_o \quad . \tag{E11}$$

In Eqs. (E10-E23), subscripts indicate partial differentiation.

2. Variance in Acoustic Velocity.

The acoustic velocity, given by Eq. (3.11), is

$$c = DY\rho_o\rho^{-1} \quad , \tag{E12}$$

and its variance is

$$V(c\ ;\ Y) = c_D^2\, V(D) + c_\rho^2\, V(\rho) \quad , \tag{E13}$$

where

$$c_D = Y\rho_o\rho^{-1} \quad , \quad c_\rho = -c/\rho \quad , \quad V(D,\rho) \equiv 0 \quad . \tag{E14}$$

3. Variance in Particle Velocity.

The particle velocity, given by Eqs. (E1) and (3.12), is

$$u = D(AY^2 + B) \quad , \tag{E15}$$

and its variance is

$$V(u\ ;\ Y) = u_D^2\, V(D) + u_A^2\, V(A) + u_B^2\, V(B) + 2u_A u_B\, V(A,B) \quad , \tag{E16}$$

where

$$u_D = u/D \quad , \quad u_A = DY^2 \quad , \quad u_B = D \quad ,$$

$$V(D,A) = V(D,B) = 0 \quad . \tag{E17}$$

4. Variance in Pressure.

The pressure, given by Eqs. (E1) and (3.13), is

$$p = \rho_o D^2(2AY^3/3 + A/3 + B) \tag{E18}$$

and its variance is

$$V(p\ ;\ Y) = p_D^2\, V(D) + p_A^2\, V(A) + p_B^2\, V(B) + 2p_A p_B\, V(A,B) \, , \tag{E19}$$

where

$$p_D = p/D \quad , \quad p_A = \rho_o D^2(2Y^3 + 1)/3 \quad , \quad p_B = \rho_o D^2 \quad . \tag{E20}$$

5. Variance in Gamma.

Gamma, given by Eq. (3.14), is

$$\gamma = Y^2/(\tilde{\rho}\tilde{p})^{-1} \tag{E21}$$

where $\tilde{\rho} = \rho/\rho_o$ and $\tilde{p} = p/\rho_o D^2$. The variance in gamma is

$$V(\gamma\ ;\ Y) = \gamma_A^2 V(A) + \gamma_B^2\, V(B) + 2\gamma_A\gamma_B\, V(A,B) \quad , \tag{E22}$$

where

$$\gamma_A = -\gamma\,[(2Y - 1)\,\tilde{\rho} + (2Y^3 + 1)/3\tilde{p}] \quad ,$$

$$\gamma_B = -\gamma\,(\tilde{\rho} + \tilde{p}^{-1}) \quad . \tag{E23}$$

In Table 3-II we list σ_{AB} and σ_D which are defined, say for p, as

$$\sigma_{AB}(p\ ;\ Y) \equiv V(p\ ;\ Y)^{\frac{1}{2}} \quad \text{when} \quad V(D) \equiv 0 \quad , \qquad (E24)$$

and

$$\sigma_D(p\ ;\ Y) \equiv V(p\ ;\ Y)^{\frac{1}{2}} \quad \text{when} \quad V(A) = V(B) \equiv 0. \qquad (E25)$$

The total standard deviation is simply

$$\sigma(p\ ;\ Y) = (\sigma_{AB}^2 + \sigma_D^2)^{\frac{1}{2}} \quad , \qquad (E26)$$

for a given fitting form. At the detonation front the total standard deviation is $\sigma(p\ ;\ 1)$ and at the end of the Taylor wave it is $\sigma(p\ ;\ Y_T)$.

APPENDIX F. STATISTICAL F TEST

The question of whether each data set comes from the same population is investigated using a statistical F test.[21] The procedure is to fit all the data sets collectively with a given fitting form denoting the sum of the squares of the deviations by $Q_o + Q_1$. This is referred to as the "restricted" model. Next, we select a particular data set and refit the remaining data sets collectively and the selected data set separately. The combined sum of the squares of the deviations from these last two fits we denote by Q_o and refer to this model as "unrestricted." We now form the quantity U given by

$$U = \frac{(n - N)}{r} \frac{Q_1}{Q_o} \quad , \qquad (F1)$$

where n and N are the number of data points and parameters respectively in the unrestricted model. The quantity $(n - N)$ is the number of degrees of freedom. The difference between the number of degrees of freedom in the restricted and unrestricted models is denoted by r. The quantity U is distributed approximately as $F(r, n - N)$.

Only the data points in the region $(Y \geq 0.515)$ are considered, since this test was performed at an early state of the investigation when the terminal characteristic was thought to be $Y = 0.515$. There are 55 data points. The point 1,1 is not considered a data point, since the fitting form is chosen a priori to pass through this point. The fitting form

$$y = (Y^B - 1)/AB + 1 \qquad (F2)$$

is used throughout the test. The results are listed in Table F-I and indicate that data set NW-432 is not a representative set.

TABLE F-I. RESULTS OF THE STATISTICAL F TEST

Restricted Model		Unrestricted Model					
Degrees of Freedom	$Q_o + Q_1$	Data Set	n-N	Q_o	r	U	F at 99%[a]
53	27.34×10^{-5}	432	51	17.34×10^{-5}	2	14.71	5.05
48	15.05×10^{-5}	442	46	13.74×10^{-5}	2	2.19	5.10
48	15.05×10^{-5}	439	46	13.74×10^{-5}	2	2.19	5.10
48	15.05×10^{-5}	435	46	14.25×10^{-5}	2	1.29	5.10
48	15.05×10^{-5}	434	46	14.72×10^{-5}	2	0.52	5.10
48	15.05×10^{-5}	433	46	12.41×10^{-5}	2	4.89	5.10
48	15.05×10^{-5}	431	46	14.30×10^{-5}	2	1.21	5.10
48	15.05×10^{-5}	430	46	12.41×10^{-5}	2	4.89	5.10
48	15.05×10^{-5}	428	46	14.13×10^{-5}	2	1.50	5.10
48	15.05×10^{-5}	427	46	14.34×10^{-5}	2	1.15	5.10

(a) F values from Ref. 22.

REFERENCES

1. A. N. Dremin and P. F. Pokhil, Dolk. Akad Nauk, USSR, 128, 899 (1959).

2. J. C. Clark, J. Appl. Phys. 20, 363 (1949).

3. C. Fauquignon, M. Prouteau, and G. Verdes, The Fourth Symposium (International) on Detonation (U. S. Naval Ordnance Laboratory, White Oak, Maryland, 1965) p. 39.

4. Douglas Venable and T. J. Boyd, Jr., ibid. p. 639.

5. R. Courant and K. O Friedricks, Supersonic Flow and Shock Waves (Interscience, New York, 1948), p. 211.

6. G. I. Taylor, Proc. Roy. Soc. (London) A200, 235 (1950).

7. W. E. Deal, Phys. Fluids 1, 523 (1958).

8. C. L. Mader, Los Alamos Scientific Laboratory Report, LA-2900 (1963).

9. E. L. Lee, H. C. Hornig, J. W. Kury, Lawrence Radiation Laboratory Report, UCRL-50422 (1968).

10. B. G. Craig, Tenth Symposium (International) on Combustion (The Combustion Institute, 1965) p. 863.

11. Bernard Hayes, J. Appl. Phys. 38, 507 (1967).

12. J. von Neumann, Collected Works (Pergamon Press, Ltd., Oxford, 1963) Vol. 6, p. 203.

13. R. E. Duff and E. Houston, J. Chem. Phys. 23, 1268 (1955).

14. W. E. Deal, J. Chem. Phys. 27, 796 (1957).

15. C. L. Mader, (comment to be published) in Proc. Fifth Symposium (International) on Detonation.

16. W. C. Davis and Douglas Venable, (to be published) in Proc. Fifth Symposium (International) on Detonation.

17. D. H. Edwards, T. G. Jones, and B. Price, J. Fluid Mech. 17, 21 (1963).

18. D. R. White, Phys. Fluids 4, 465 (1961).

19. W. W. Wood, Phys. Fluids 6, 1081 (1963).

20. J. J. Erpenbeck, Phys. Fluids 7, 1424 (1964).

21. F. A. Graybill, Introduction to Linear Statistical Models (McGraw-Hill, 1961), p. 135.

22. A. Hald, Statistical Tables and Formulas (John Wiley and Sons, Inc., New York, 1952, p. 54.

McD/tc: 381 (100)